ELSEVIER

Journal of Hazardous Materials A132 (2006) 119–140

Journal of Hazardous Materials

www.elsevier.com/locate/jhazmat

Review

A review of large-scale LNG spills: Experiments and modeling

Anay Luketa-Hanlin *

Sandia National Laboratories, Fire Science and Technology Department, P.O. Box 5800, MS-1135 Albuquerque, NM 87185, USA

Received 21 April 2005; received in revised form 30 September 2005; accepted 4 October 2005
Available online 4 November 2005

Abstract

The prediction of the possible hazards associated with the storage and transportation of liquefied natural gas (LNG) by ship has motivated a substantial number of experimental and analytical studies. This paper reviews the experimental and analytical work performed to date on large-scale spills of LNG. Specifically, experiments on the dispersion of LNG, as well as experiments of LNG fires from spills on water and land are reviewed. Explosion, pool boiling, and rapid phase transition (RPT) explosion studies are described and discussed, as well as models used to predict dispersion and thermal hazard distances. Although there have been significant advances in understanding the behavior of LNG spills, technical knowledge gaps to improve hazard prediction are identified. Some of these gaps can be addressed with current modeling and testing capabilities. A discussion of the state of knowledge and recommendations to further improve the understanding of the behavior of LNG spills on water is provided.

Keywords: LNG; Liquefied natural gas; Review; Experiment; Modeling; Hazards

Contents

* Tel.: +1 505 284 8280; fax: +1 505 845 3151.
E-mail address: aluketa@sandia.gov.

0304-3894/$ – see front matter © 2005 Elsevier B.V. All rights reserved.
doi:10.1016/j.jhazmat.2005.10.008

1. Introduction

Recently there has been considerable interest concerning possible risks associated with the storage, handling, and transportation of liquefied natural gas (LNG) due to plans to widely expand the LNG market by building several new receiving terminals in the U.S. and concerns of terrorist attacks. Due to the large volume of LNG potentially involved, the hazards are large-scale and consequently accurate hazard prediction can be difficult.

In order to best address hazard predictions, experimental, numerical, and analytical efforts must be combined. An extensive experimental effort was performed in the 1970s and 1980s pertaining to the behavior of LNG when spilled on water, with and without subsequent ignition. Recently, with the renewed interest and concerns regarding LNG shipping, there have been several analytical studies addressing the possible consequences associated with an LNG spill on water [1–6]. These studies have provided significantly differing results, partly due to the uncertainties of parameter values necessary for hazard prediction, and partly due to differences in modeling approaches and assumptions.

This paper reviews the experimental work done on large-scale spills of LNG, as well as some of the modeling and analytical work performed. This review is motivated by the need to determine the current gaps and limitations in understanding and predicting the hazards associated with these large-scale spills.

There are currently four import terminals in the U.S. and at least three dozen proposals to build new terminals over the next several years. By 2010, the new terminals are projected to import a total of 23 billion m^3 (812 billion ft^3) annually. The four U.S. LNG import terminals currently have an estimated combined peak capacity of 34 billion m^3 (1.2 trillion ft^3) per year and an estimated base load capacity of 25 billion m^3 (880 billion ft^3) per year. The U.S. imported approximately 14 billion m^3 (505 billion ft^3) of LNG in 2003 [7].

LNG transport is most often by ship. LNG ships are roughly 300 m (1000 ft) in length, double-hulled and have holding capacities between 125,000 and 160,000 m^3 (4.4 and 5.7 million ft^3). Larger ships up to 250,000 m^3 (8.8 million ft^3) holding capacities are currently being considered for construction. The volume is distributed among four to six individual insulated tanks where the LNG is kept at atmospheric pressure and 111 K (−260 °F). LNG is comprised mostly of methane (85–95 vol.%) with ethane, propane, and small amounts of other heavier hydrocarbons comprising the rest. Once it is transported to a receiving terminal it is stored in heavily insulated tanks and then regasified for distribution via the pipeline system to consumers.

The potential hazards associated with LNG are varied. These include cryogenic tissue damage caused by direct contact, pressure due to rapid phase transitions (RPTs), deflagrations, detonations, vapor cloud fires and pool fires. Due to its extremely cold temperature, direct contact will result in severe tissue damage and embrittlement to materials. Since LNG vapors displace air, asphyxiation is possible, as well as lung damage from breathing cold vapors. When LNG comes in contact with water at a temperature significantly above the boiling point of LNG there is the possibility of rapid phase transition, a non-combusting type of explosive expansion. These vapor expansions can produce significant overpressures that can result in structural damage. There are also thermal hazards from different combustion events such a pool fire, vapor cloud fire, and explosion.

To gain an understanding of the information necessary for hazard prediction, it is instructive to go through the evolution of a spill from a LNG ship. Fig. 1 provides a simplified representation of a spill and the possible outcomes that can result. Determining the amount of LNG spilled is a necessary first step in predicting the possible hazards. In the event of a breach of one of the four to six tanks on a vessel, the hole can occur either above or below the waterline. The rate at which LNG flows from the breach must be determined and will depend upon the shape of the tank and the size, level of fill, and location of the hole.

LNG is roughly half the density of water and at its boiling point the vapor is 1.5 times the density of air. LNG will float on water and due to the high heat transfer between it and the water

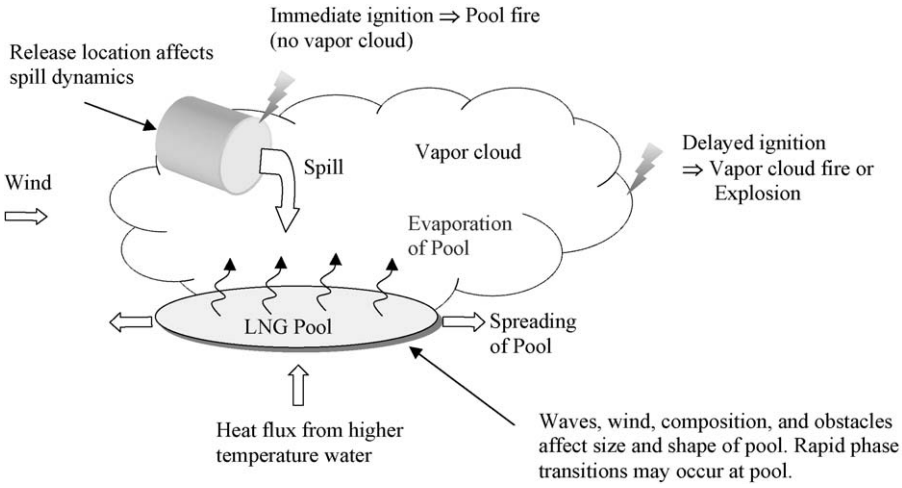

Fig. 1. LNG spill over water.

will rapidly vaporize forming a low lying visible cloud due to the condensation of entrained water vapor in the atmosphere. Once the LNG spills onto the water the pool will spread and vaporize simultaneously. The shape and size of the pool can be affected by environmental conditions, such as wind, waves, and currents. The exact extent that waves affects spreading is unknown at this time, but it would be expected that the evaporation rate would increase due to the increase in surface area and increased heat transfer from enhanced transport from turbulent motion. An increase in wind speed tends to increase the local evaporation rate as well. Wind would also cause the pool to have varying thickness. There is also the effect of currents associated with traveling waves, which could transport the pool further away from the spill than a non-wave condition. This is in contrast to a standing wave condition where the wave does not propagate through the water, but remains stationary. It would also be more likely that the waves would break up the pool into multiple, irregular shaped pools than would occur on a quiescent surface.

The composition of the LNG also affects the size of the pool. The addition of heavier hydrocarbons such as ethane and propane tend to result in an increase in the evaporation rate due to vapor film collapse to be described in Section 2.1, thereby resulting in a smaller pool. RPTs can also occur at the pool causing an increase in the vaporization rate.

If released LNG ignites immediately, a pool fire will result. If not immediately ignited, the LNG will rapidly vaporize to produce a low-lying visible cloud, which will spread at roughly the wind speed. LNG vapor is colorless, but due to its very low temperature, entrained water vapor in the atmosphere is condensed and produces a visible cloud. Although LNG is comprised of several components, methane will boil off first since it is the lightest component. Thus, the cloud will initially be comprised of methane. Near the end of evaporation, the heavier hydrocarbons will boil off and will then comprise an increased fraction of the cloud, though methane will still comprise the majority.

The cloud that forms will mix with air, principally at the cloud edges, and when concentrations of methane reach between the lower and upper flammability limits (LFL and UFL), 5–15% by volume, the mixture can sustain a flame if ignited. Portions of the cloud surrounding the UFL will burn as a diffusion-controlled fire. If flammable portions come in contact with an ignition source, a vapor cloud fire can result which may propagate back to the spill point to burn as a pool fire. Vapor cloud fires can burn in two principal modes as either a slow burn back, also termed a flash fire, or as a fireball, the rapid burning of fuel characterized by high upward acceleration. Fireballs occur when fuel is atomized sufficiently to provide a mixture with air that can be rapidly consumed. They are more likely with a large rapid release of fuel resulting from a high momentum impact source. Fireballs are short duration events, on the order of seconds, but are still lethal within close proximity. If the vapor cloud reaches a location with some confinement and sufficient mixing with air, an explosion in the form of a deflagration with damaging overpressures may result. In some special cases, with high degrees of confinement, strong mixing with air, and large ignition sources, a detonation may be possible.

Thus, in order to analyze combustion events, it is necessary to consider pool fires, vapor cloud fires, and explosions. The factors that are involved in calculating the hazards from a pool fire are flame geometry including pool size and shape, burn rate, heat radiated, and view factor. For vapor cloud fires the extent of the cloud, its composition, and radiative properties are required for analysis. Explosions require knowledge of the degree of mixing of various species, extent of confinement as well as the characteristics of the ignition source, such as its strength and geometry.

This description of the possible outcomes of a spill gives an indication of the various parameters necessary for hazard prediction. Thus, experimental studies have been concerned with obtaining data on the dispersal of LNG vapor clouds and on different combustion modes such as pool fires, vapor cloud fires, and explosions. The following reviews large-scale experiments on the behavior of a disperse LNG cloud, and large scale fire studies of LNG spills on water and land. Large in the context of this paper refers to the largest tests to date. Typically, the largest tests have had pool diameters 10 m or greater and require field rather than laboratory testing. Models used to predict dispersion distances and thermal hazards are also described and discussed. Since the evolution of a LNG vapor cloud and related hazards

are strongly influenced by characteristics of the pool that forms from a spill, discussion on spreading, boiling, and rapid phase transitions of the liquid pool is provided. Areas in which technical knowledge gaps exist on hazards related to LNG spills on water are discussed, and recommendations on addressing these areas via experimental testing and simulation to improve hazard prediction are provided.

2. Pool formation

For unconfined LNG spills on water, the LNG spreads and boils at a very high rate. The high vaporization rate is constantly maintained due to continual contact with much higher temperature water. If the spill is confined on calm water, then the prevention of spreading may result in the formation of an ice layer beneath the LNG. As the ice layer thickness increases, the heat transfer rate decreases, thereby reducing the evaporation rate. The boiling rate would then be similar to confined spills on land in that the evaporation rate decreases with time [8]. Small amounts of ice formation has been observed in unconfined spills on water, but during spreading the turbulent interface created between the LNG and water, as well as the large heat source provided by the water, prevents significant ice formation. Once the LNG has spread to its maximum area, the thickness of the LNG (∼1 mm) is not sufficient to provide enough thermal inertia to freeze significant amounts of water.

Higher vaporization rates result in a greater distance to LFL, which affects the extent of vapor cloud fire and explosion hazards. An increase in vaporization rate will also increase the total burn rate since the heat transfer from the water and fire both contribute. An increase in burn rate will decrease the pool area, thereby reducing the size of a pool fire. Although a smaller pool fire results, a taller flame occurs due to the increased burn rate. The shape of the pool will also determine the thermal hazard distances from a pool fire. Thus, determining the vaporization rate, as well as the shape and size of the pool is instrumental for hazard prediction. The following Sections 2.1–2.3, provide a description and discussion of experiments and modeling of factors that affect the formation of an LNG pool.

2.1. Pool boiling experiments and modeling

Pool boiling occurs when LNG is spilled onto water due to the high temperature difference of roughly 180 K (325 °F). Modes of pool boiling and corresponding heat transfer rates are a function of temperature difference. This relationship can best be described by discussing a heated surface immersed in a liquid and the heated surface brought to a surface temperature at the boiling point of the liquid. At this temperature, vapor formation or boiling occurs and is termed the regime of nucleate boiling, where nucleation sites (gas or vapor-filled cavities) on the surface develop to allow vapor bubbles to form. Although nucleation is usually considered to occur at a solid surface, it can also occur in a homogenous liquid.

With a further increase in surface temperature, the bubble formation rate increases, producing high local velocities within the liquid film next to the surface, thereby enhancing the heat transfer. Thus, in this regime an increase in temperature difference will increase the heat transfer to the liquid. A peak heat flux occurs in the nucleate boiling regime. Eventually, the bubble formation is so rapid the liquid is prevented from contacting the surface and the heat flux decreases. This is the transitional regime.

With further increases in surface temperature a continuous vapor film will cover the surface and the heat transfer will be reduced since heat is transferred poorly across the low-conductivity vapor film. This regime is called film boiling and the minimum temperature for stable film boiling is called the Leidenfrost temperature. A minimum film boiling heat flux occurs at this temperature. With further increases in temperature the mode of heat transfer becomes radiative and the heat transfer increases, though most materials fail at this point.

Since LNG is a mixture of hydrocarbons of different molecular weights, evaporation will take place preferentially, in that boil off occurs according to the molecular weight of the fuel. Thus, methane will boil off first since it has a lower molecular weight than ethane and propane. This process leading to enrichment of LNG with the heavier hydrocarbons is sometimes referred to as 'ageing' or 'weathering' in the industry. The boiling heat flux for mixtures can be very different than for individual components of the mixture. Ethane and propane have higher boiling points, 185 K (−127 °F) and 231 K (−44 °F), respectively, than methane at 111 K (−260 °F). Film boiling occurs for pure liquefied methane on water, but with the addition of ethane and propane boiling will occur in either the nucleate or transitional regime principally in the later stages of the evaporation of the pool, though this mode of boiling can occur any time during evaporation when there is contact with the water and enriched regions. Experimental and modeling studies have demonstrated that chemical composition affects the vaporization rate of LNG, and thus should be included in evaporation models.

Boe [9] performed laboratory scale experiments with liquefied methane–ethane and methane–propane mixtures boiling on water. The results indicated that addition of ethane or propane affects the boil off rate. High initial boil off rates were observed for methane rich mixtures similar to that of typical LNG compositions. Boil off rates increased by a factor of 1.5–2 from that of pure methane when either ethane or propane was added for a 97% methane mixture. It was concluded that there is a break down of film boiling due to closer contact between the mixture and water causing a higher heat flux and lower temperature difference below that to maintain a continuous vapor film.

Results by Drake et al. [10] on laboratory scale experiments showed that LNG had a higher boiling rate than pure methane on an unconfined surface. Light LNG compositions of 98% methane and 2% ethane were tested, as well as heavy compositions, 82–89% methane with ethane-propane ratios between 4 and 5. Increasing the amount of heavier hydrocarbons resulted in more rapid vaporization. The rate of boiling increased with time and foaming of the LNG on the water surface occurred. These results agree with Valencia-Chavez and Reid [11] on laboratory scale confined spills.

Conrado and Vesovic [12] developed a model to investigate the influence of chemical composition on the spill behavior of

LNG and LPG for unconfined water surfaces. Spreading based upon a gravitational-inertia balance, heat transfer, and vaporization was included in the model. They point out that preferential evaporation occurs and that boiling does not take place at a constant temperature. They found that a decrease in the rate of vaporization due to the change in composition of the pool occurs in the later stages of the pool. The vaporization rate for LNG (90% methane, 10% ethane) versus methane was found to be different. By not considering preferential boil-off this would result in underestimating the evaporation time by about 20%. For instantaneous spills, results indicate that neglecting evaporation while spreading is a reasonable assumption. They conclude that models should use the properties of LNG that reflect all compounds and not that of pure methane.

2.2. Rapid phase transition experiments and modeling

Rapid vapor expansions are termed rapid phase transitions in the LNG industry. They can occur when the very cold LNG comes in contact with water. These expansions are not combustion related, but rather are classified as a physical or mechanical expansion where there is a high-pressure energy release. Vapor steam expansions have been extensively studied in the nuclear power industry and in the industrial process industry such as foundries. Research on LNG/water expansions has been principally at laboratory scale [13–15].

The Coyote test series [16–21] performed by LLNL has been the only large-scale test explicitly for the study of RPTs. These tests also had the objective of studying the behavior of LNG vapor cloud fires to be described in Section 4.1.1.3. The Coyote series was a continuation of the Burro test series [22,23], to be described in Section 3.1.4, to further study combustion hazards and RPTs. They were performed by LLNL and the Naval Weapons Center at China Lake, California and sponsored by the U.S. DOE and the Gas Research Institute. To study RPTs, 13 spills of 3–14 m^3 (106–494 ft^3) with flow rates of 6–19 m^3/min (212–671 ft^3/min) were performed with fuel of varying ratios of methane, propane, and ethane, with methane concentrations between 75 and 92% by volume.

Six of the 18 Coyote spills produced RPTs. Most were early RPTs that occurred immediately with the spill, and in some cases, continued for the duration (over a minute) of the spill. They were generally located near the spill point and appeared to be primarily underwater. Delayed RPTs, occurring at the end of the spill and located away from the spill point out on the LNG pool surface, were also observed. Delayed RPTs occurred in three tests.

It has been shown that much different behavior occurs at larger scales, which was not predicted from smaller scale studies. Enger and Hartman [24] from Shell performed a series of small-scale experiments on the order of 0.1 m^3 (3.5 ft^3) on RPT formation and found that the methane content of LNG must be less the 40 mol% (~35 vol.%) for RPTs to occur. The Coyote tests found RPTs can occur with methane rich mixtures up to 88% by volume, indicating that other mechanisms become dominant for larger spills. It was also found that even when there were similar compositions, RPTs may or may not occur. Thus, the pre-spill composition is not the only factor determining the occurrence of RPTs.

The occurrence of RPTs appeared to correlate with water temperature and the depth of penetration of the LNG into the water. RPTs occurred when the water temperature was above 290 K (63 °F), though when an adjustable spill plate, used to prevent the LNG from impinging upon and eroding the pond bottom, was removed allowing for deeper penetration into the water RPTs resulted even though the water temperature was 285 K (52.9 °F).

The strength of RPT's was found not to correlate with impact pressure. This is in contrast to what was found for laboratory-scale spills by Jazayeri [25] in which cryogens were impacted with water and a correlation was found between RPT strength and impact pressure.

The strength of the RPT was found to correlate with spill rate. An abrupt increase in the RPT strength yield was found at around 15 m^3/min (530 ft^3/min), and at around 18 m^3/min (636 ft^3/min) the strength increased by five orders of magnitude. The maximum equivalent free-air, point source TNT explosion that occurred was 6.3 kg (14 lb) for an 18 m^3/min (636 ft^3/min) spill rate. This is believed to be a significant underestimation of the actual energy released since the majority of the blast was directed underwater.

RPTs were also found to increase the distance to LFL by as much as 65% due to the increase in vaporization rate from the expansion. The RPTs that occurred late in the spill resulted in ethane enrichment of 40% by volume in the RPT 'puffs' due to the higher concentration of ethane in the LNG on the pond. Ethane has an LFL of 3%, and consequently the distance to LFL was increased by about 60% for these regions.

Several theoretical models have been proposed to explain the formation of rapid phase transitions, though none have addressed the large-scale behavior observed in the Coyote experiments. There are several recent reviews of the various theories proposed to explain similar phenomena for steam expansions [26–28].

The prevalent theory is the superheat theory which proposes that immediately after LNG is spilled on water film boiling occurs. Then due to possible instabilities and a decrease in the temperature difference the film boiling vapor layer collapses in localized areas resulting in liquid/liquid contact. This direct contact results in rapid vaporization from the increased heat transfer so that a pressure wave is produced to achieve a rapid expansion. For a rapid phase transition to occur, the water has to be equal or slightly greater than the superheat temperature of LNG ($T_{superheat} < T_{water} < 1.1T_{superheat}$). Superheat temperature for methane, ethane, propane, and butane are 168, 269, 326, and 376 K (−157, 24.5, 127, 217 °F), respectively [29]. The superheat temperature of hydrocarbon mixtures is approximately the mole fraction average of the superheat temperatures of the components [30].

Napier and Roochland [31] raise the issue of rapid phase transitions causing ignition by either electrostatic discharge or frictional sparks created near the rapid phase transition, or by shock-heating of the methane–air mixture. Based on shock tube analysis, they concluded that shock-heating of unconfined flammable mixtures of methane to the auto ignition temperature

(813 K) (1004 °F) is not possible. The experimentally determined temperature available is 450 K (350 °F), theoretical is 500 K (440 °F). They state that ignition is possible via an electrostatic discharge or frictional sparks, but these ignition modes are difficult to quantify, though in the near vicinity of an RPT, blast damage can occur which could result in ignition from these modes.

2.3. Experiments and modeling of LNG spreading on water

There have been several small-scale experiments reporting mass flux and pool spread for LNG spills on water, but few large-scale experiments have provided such information since their objective has been dispersion and combustion characteristics of the vapor cloud. Table 1 provides a list of experiments that have provided pool radius and mass flux values from an unignited pool. Experiments have used markers in the pool and photography above the pool to record the spread rate and size of the pool over time. From knowledge of spill rate and pool area, an average mass flux can be determined. There is a high degree of uncertainty in this method since the pool area may become irregular due to wind, thereby making the area difficult to determine. In addition, a visual of the liquid pool overhead is difficult due to vapor blocking. Thus, very detailed comparison of experimental and model results is not possible with currently available data.

There have been several models developed for the spread of LNG on water [32–39]. Otterman [32] and Briscoe and Shaw [34] provide model-to-model comparison for spills on the order of 10^3 to 10^4 m^3 ($3.5–35 \times 10^4$ ft^3). The majority of models assume that the pool is circular and that spreading is driven only by gravity, and ignore the action of waves and currents, preferential boiling, and pool break-up. The following models are typical approaches used to represent the spread of LNG on water.

Opschoor [39] developed a model for the spread and evaporation of LNG on open and confined quiescent water surfaces. For an unconfined water surface the model assumes that boiling occurs in the film-boiling mode and that no ice formation occurs. For confined water surfaces, the model assumes that during the spreading phase no ice formation occurs due to film boiling, and that after spreading an ice layer forms due to a decrease in temperature difference between the LNG and water. The results were compared with experiments by Boyle and Kneebone for spills of 38 kg (84 lb) [40]. There was agreement with evaporation rate for confined water surfaces for the ice formation period, and fair agreement for unconfined water surfaces for pool radius. When compared to experiments by U.S. Bureau of Mines [41,42] for spills of 163 kg (359 lb) the model under-predicts the pool radius over time.

Waite et al. [43] incorporates heat transfer, preferential boil off of methane (90%) and ethane (10%), and gravity spreading of the pool. Assuming a heat flux typical for film boiling of about 25 kW/m^2 (7.93×10^3 Btu/h ft^2), the model had fair agreement to within 20% on the pool radius found in the experiments by U.S. Bureau of Mines [41,42] and Boyle and Kneebone [40]. This heat flux value gave better agreement than the heat flux typically assumed of 100 kW/m^2 (3.17×10^4 Btu/h ft^2).

Brandeis and Ermak [44] developed a numerical model based on the depth-averaged, shallow water equations. Instantaneous and continuous spills that included the effect of mass and heat transfer, shear forces, and surface tension were modeled. Pool break-up was treated by including the effect of shear forces and surface tension. It was found that the time necessary to reach a steady-state radius for continuous spills increased with increasing surface shear stress. The steady-state pool radius was not affected. The results were compared to experiments performed by Boyle and Kneebone [40] on a 0.0817 m^3 (2.89 ft^3) spill, and indicated good agreement.

Cavanaugh et al. [45] developed a code LSM90 that simulates multi-component spills on land or water that accounts for flashing liquid, entrainment as aerosol, liquid pool evaporation, and heat and mass transfer effects. Spreading is driven by gravity and the actions of waves are not modeled. Results were compared to the Esso [46,47] and Burro [22–23] series of experiments to be described in Sections 3.1.1 and 3.1.4, respectively. The difference between experimental and computed results for evaporation rate varied from 1 to 48% with 8 out of 10 cases within 14%. The average difference for pool size comparison was 12%. The spill size for which the comparison was made was not stated.

3. Vapor dispersion of LNG spills on water

For unconfined spills on water, the cloud will travel at roughly the wind speed before becoming buoyant and dispersing. Initially the temperature of the LNG vapors will be close to the pool temperature and thus will be denser than the surrounding air. Natural gas vapors must be at 166 K (−160 °F) to be neutrally buoyant in air at 289 K (60 °F). The duration that the cloud will persist will usually be on the order of 10 s of minutes. For

Table 1
LNG experiments on water with measurement on pool radius and mass flux[a]

Experiment	Spill volume (m^3)	Pool radius (m)	Mass flux (kg/m^2 s)
Boyle and Kneebone [40]	0.023–0.093 (pond)	1.97–3.63	0.029
Burgess et al. [41–42]	0.0055–0.36 (pond)	.75–6.06	0.181
Feldbauer et al. (ESSO) [46–47]	0.73–10.2 (Matagorda Bay)	7–14	0.195
Maplin Sands [52–55]	5–20 (inlet surrounded by 300 m dyke)	∼10	0.085
Koopman et al. (Avocet LLNL) [56]	4.2–4.52 (pond)	6.82–7.22	0.12

[a] Some experiments report evaporation rates in units of m/s. Mass flux values were obtained by multiplying evaporation rates by an assumed density of 450 kg/m^3 for LNG.

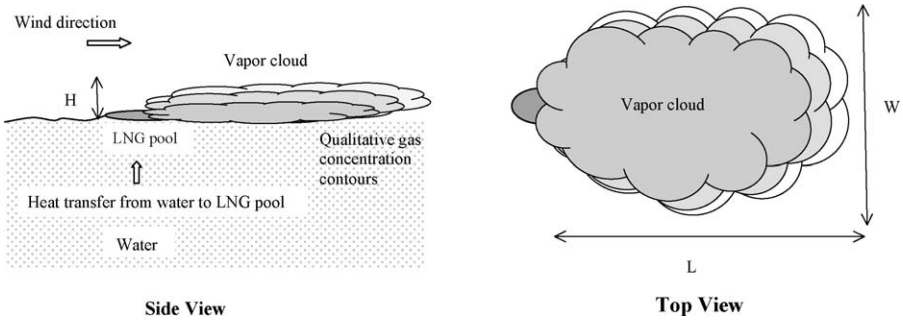

Fig. 2. Typical vapor cloud shape in wind for an LNG spill on water.

land-based storage facilities with barriers, dense gas behavior is advantageous since the vapor is more easily contained, however this does have the disadvantage that the LNG vapor will persist for a longer period of time.

Fig. 2 provides an indication of the general shape of an LNG vapor cloud in wind. The length of the cloud will usually be much greater than its width due to wind elongating the cloud, although for low wind speeds, around 1–2 m/s (2–4.5 mph), the length and width will be roughly similar. The ratio of L/W will typically be around 5 for higher wind speeds. The cloud has a very low height (~10 m) relative to it length and/or width. The ratio of L/H will typically be on the order of 100. Gas concentrations vary throughout the cloud as qualitatively indicated in Fig. 2. The highest concentrations will occur near the spill and then will decrease to reach the lower flammability limit at the peripheral regions of the cloud.

Table 2 provides a list of LNG dispersion field tests of spills on water and the respective maximum measured distance to the LFL of methane. The spill volumes and rates listed in Table 2 indicate that both are important factors in affecting the distance to LFL. The distance that the cloud will travel will also depend upon the vaporization rate of LNG, the presence of obstacles, and atmospheric conditions, such as wind velocity, humidity, and atmospheric stability, as well as mode of release, including aspects such as above or below waterline. Conditions that enhance mixing of the cloud with air and/or the cloud's buoyancy will reduce the distance to the LFL. Obstacles and rough terrain will also tend to reduce the distance to the LFL, as does high humidity, and less stable atmospheric conditions. It has been found experimentally that in general low wind speeds and highly stable atmospheric conditions will result in the greatest distance to LFL. An underwater release would result in a more buoyant cloud due to the enhanced heat transfer from the passage of the rising LNG through the water, thereby resulting in a reduced distance to LFL.

The following section describes experiments on the dispersion characteristics of vapor clouds formed from unconfined LNG spills onto water. Only the largest spill volume tests are reviewed and discussed. Smaller spill volume tests have been performed and are listed in the recent review on cryogenic spills by Thyer [48]. A comprehensive listing of LNG experiments and description of processes related to LNG operations is provided by Lees [49]. Additional description and discussion of LNG fire, dispersion, and RPT experiments and modeling performed up to 1982 is provided in [50].

3.1. Experiments

3.1.1. Esso [1973]

Tests were conducted under contract by the Esso Research and Engineering Company and the American Petroleum Institute in Matagorda Bay, Texas [46–47]. Volumes ranging from 0.73 to 10.2 m^3 (26–373 ft^3) were spilled at a flow rate of 18.9 m^3/min (671 ft^3/min). It was observed that LNG vapor clouds are visible and are very low in height compared to their lateral extent. Calculations of the density of mixtures of air at 294 K (70 °F) and methane at 111 K (−260 °F) at different humidity levels indicated that the density of the LNG vapor–air mixture is affected by atmospheric humidity where increasing humidity results in lower density mixtures. Variation in the LNG composition for the range tested, 85–94% methane, did not have a significant effect on downwind concentrations. In one test, a delayed rapid phase transition occurred.

Table 2
LNG dispersion tests on water

Experiment	Spill volume (m^3)	Spill rate (m^3/min)	Pool radius (m)	Downwind distance to LFL (m) (max)
ESSO [46–47]	0.73–10.2	18.9	7–14	442
Shell [51]	27–193	2.7–19.3	NA (jettisoned)	2250[a](visual)
Maplin Sands [52–55]	5–20	1.5–4	~10	190 ± 20
Avocet (LLNL) [56]	4.2–4.52	4	6.82–7.22	220
Burro (LLNL) [22–23]	24–39	11.3–18.4	~5	420
Coyote (LLNL) [16–21]	8–28	14–19	Not reported	310
Falcon (LLNL)[b] [57]	20.6–66.4	8.7–30.3	Not reported	380

[a] Total extent of the cloud (maximum LFL distance not measured). Thus, maximum distance to LFL is less than this value.
[b] Vapors were partially contained within a vapor fence.

A range of pool radii, 7–14 m (23–46 ft), was visually observed, and the vaporization mass flux was calculated to be approximately 0.195 kg/m^2 s (.040 lb/ft^2 s). The maximum distance to LFL measured by hydrocarbon sensors was roughly 442 m (1450 ft) for a spill size of 7.12 m^3 (253 ft^3) and wind speed of 4.9 m/s. There were some spills for which the cloud exceeded the array of sensors thus the distance to LFL was not measured. The longest distance to the last visible fog from the spill site was 1372 m (4500 ft) for a spill size of 8.37 m^3 (297 ft^3) and wind speed of 4 m/s (9 mph).

3.1.2. Shell Jettision Tests [1973]

Shell performed a series of six tests in which LNG was jettisoned from 'Gadila', a 75,000-m^3 (2.7×10^6 ft^3) capacity ship, at a location about 70 miles west of St. Nazaire, France [51]. These tests involved the largest volume of LNG released over water to date. The primary objective of the tests were to determine the feasibility of emergency jettison of fuel with high discharge rates while the ship is stationary, as well as low discharge rates while the ship is moving. The flow rates tested ranged from 2.7 to 19.3 m^3/min (96–685 ft^3/min), lasting ten minutes to give total volumes spilled from 27 to 193 m^3 (960–6850 ft^3). Four tests were performed while the ship was moving from 1.5 to 5.4 m/s (3–10.5 knots), and two stationary tests were performed, one of which was with the highest volume spilled. LNG was jettisoned from two different jet nozzle sizes, 51 and 102 mm (2 and 4 in.) located 18 m (59 ft) above the water, in wind speeds ranging from 1.9 to 5.1 m/s (4.3–11 mph).

Concentration measurements were not taken, but the extent of the visible cloud was observed using overhead cameras. Infrared camera results indicated that, with the 51 mm (2 in.) nozzle, LNG pools on the sea surface did not form and only isolated patches formed using the 102 mm (4 in.) nozzle. This result could be due to the LNG evaporating before it reached the sea surface since it was released from a horizontal jet elevated 18 m (59 ft) above the waterline. Thus, ice formation or RPTs were not observed. Also, no significant static charges that could serve as ignition sources were generated in the jet.

The dense vapor cloud completely dispersed within 5–10 min after the end of discharge using the 51 mm (2 in.) nozzle, and with 15–20 min using the 102 mm (4 in.) nozzle. For the highest volume spilled, 193 m^3 (6850 ft^3) in a 3.9 m/s (8.7 mph) wind, the visible plume appeared to be uniform over its entire length and had a height of 10–12 m (33–39 ft), maximum continuous width of 550 m (1800 ft), and length of 2250 m (7400 ft).

The main conclusion from the study was that LNG could be jettisoned without the vapor cloud engulfing the ship, and without LNG contacting the ship to result in cryogenic damage.

3.1.3. Maplin Sands tests [1980]

Tests were conducted at Maplin Sands, England by the National Maritime Institute and were sponsored by Shell [52–55]. These tests were performed in order to obtain dispersion and thermal radiation data on 20 spills of LNG and 14 spills of propane onto water for instantaneous and continuous spills. The results on thermal radiation data will be described in Section 4.1.1.2.

Twenty-four continuous and ten instantaneous spills were performed in average wind speeds of 3.8–8.1 m/s (8.5–18 mph). Instantaneous spills were performed by rapidly sinking a barge loaded with LNG or propane. For the instantaneous spills, the spill volumes tested were 5–20 m^3 (178–710 ft^3), and for continuous spills, spill rates were 1.5–4 m^3/min (53–141 ft^3/min). A 300 m (984 ft) diameter dyke surrounded the spill point for containment.

It was found that the dispersion behavior of the cloud was affected by the method of LNG release. For an underwater release, a more buoyant cloud resulted, whereas with an above water release, a lower and longer downwind cloud resulted. An RPT was observed in one of the instantaneous LNG spills, resulting in a maximum overpressure of 1.8 kPa (0.26 psi) and damage to the barge.

A typical pool radius was roughly 10 m (33 ft), and the evaporation rate was calculated to be approximately 2×10^{-4} m/s (6.6×10^{-4} ft/s). Pool radius as a function of spill rate was not reported. Using a 3-s average measurement, the maximum dispersion distance to LFL for a spill rate of 3.2 m^3/min (114 ft^3/min) and wind speed of 5.5 m/s (12 mph) was 190 ± 20 m (623 ± 66 ft) downwind of the spill. The distance to LFL was found to be within the visible boundary of the vapor cloud for a calculated humidity range of 50–100%.

3.1.4. Burro tests [1980]

The Burro tests were performed by Lawrence Livermore National Laboratory (LLNL) at the Naval Weapons Center at China Lake, California and sponsored by the U.S. DOE and the Gas Research Institute [22–23]. A total of 8 LNG releases onto water were performed with spill volumes ranging from 24 to 39 m^3 (848–1377 ft^3), spill rates of 11.3–18.4 m^3/min (399–650 ft^3/min), wind speeds from 1.8 to 9.1 m/s (4–20 mph), and atmospheric stability conditions from unstable to slightly stable. Dispersion occurred over water for 29 m (95 ft) from the spill point on a 58 m (190 ft) diameter pond, 1 m (3.3 ft) deep, then over land for 80 m (262 ft) where the terrain was irregular with a rise of 7 m (23 ft). Beyond this point, the land was relatively level. These tests were preceded by the Avocet series of discovery experiments for 5 m^3 (177 ft^3) spills [56]. The Avocet tests were performed in order to gain insight into the measurements necessary for the larger spills to be tested in the Burro series of experiments.

Measurements of wind speed and direction, gas concentration, temperature, humidity, and heat flux from the ground were made at several distances from the spill and at several elevations. Gas concentration measurements were averaged over 10 s durations. High-frequency data indicated that significant fluctuations about the 10 s average occurred such that the instantaneous flammable extent of the gas cloud will be larger than is indicated by the mean LFL contour.

In one of the tests, the cloud caused displacement of the atmospheric flow and resulted in the gas velocity within the cloud decreasing to almost zero. The dense cloud was able to dampen turbulent mixing by stable stratification and thus the wind was able to flow over the cloud as if it was a solid object. This test was performed under a low wind speed of 1.8 m/s (4 mph), slightly

stable atmosphere, and spill rate of 16 m^3/min (565 ft^3/min) and spill volume of 28.4 m^3 (1000 ft^3). For the other tests with higher wind speeds, this effect was not observed. The cloud was wider and lower in height than that of any other test. The maximum radial distance to LFL at 1 m (3.3 ft) elevation was approximately 420 m (1378 ft). The cloud also remained over the spill region after the spill ended, in contrast to the other tests where the cloud propagated downwind within 10–20 s after spill termination.

Differential boil-off was observed in the tests where ethane and propane enrichment up to 40% in the cloud occurred late in the spills and propagated downwind up to 140 m (459 ft). It was also found that a relative increase in absolute humidity is correlated to an increase in gas concentration. A 1% gas concentration in the cloud was associated with a 15% increase in absolute humidity. Thus, water was entrained into the cloud such that the water content of the gas cloud was substantially higher than the ambient air.

For the Burro 8 experiment, overhead photography showed most of the cloud's width to be contained within a 140 m (459 ft) arc where gas sensors arrays were placed, though part of the cloud spread past the array. Gas concentration measurements indicated that LFL was reached within the 140 m (459 ft) arc. Thus, the distance to LFL was within the visible portion of the cloud, even for an atmospheric humidity of 5%. This could be due to the entrainment of water vapor from the pond into the cloud.

RPTs also occurred in these tests producing overpressures (static) up to 5 kPa (.73 psi) measured at a distance of 30 m (98 ft) from the spill point. They were strong enough to cause damage to the spill pipe support and spill plate. In one test, an RPT caused the 27 kg (60 lb) spill plate to be thrown 50 m (165 ft) downwind. The base of the end spill pipe support structure, a 1.22 by 1.22 m (4 ft) concrete slab with a mass of almost 227 kg (500 lb), was displaced by almost 0.61 m (2 ft).

3.1.5. Falcon tests [1987]

The Falcon tests were conducted at Frenchman Flat in Nevada by LLNL and sponsored by the Gas Research Institute and the U.S. DOT [57]. The objectives of the tests were to provide a database on LNG vapor dispersion from spills involving obstacles and to assess the effectiveness of vapor fences for mitigating dispersion hazards. The testing was performed on a 40 m × 60 m (131 × 197 ft) pond enclosed by an 88 m (289 ft) long by 44 m (144 ft) wide by 9.1 m (30 ft) high vapor fence. A 22 m (72 ft) wide by 13.7 m (45 ft) high barrier was placed upwind of the pond in order to simulate the obstruction of a storage tank.

Five tests were performed with spill rates of 8.7–30.3 m^3/min (107–1070 ft^3/min), volumes of 20.6–66.4 m^3 (727–2345 ft^3), wind speeds of 1.7–5.3 m/s (3.8–12 mph), and methane concentrations of 88–94.7%. Gas concentration and temperature measurements were taken at towers upwind and downwind of the spill.

Falcon-1, the test with the highest volume, 66.4 m^3 (2345 ft^3) and spill rate, 28.7 m^3/min (1014 ft^3/min), and most stable atmospheric conditions (stability class G), resulted in the vapor cloud overfilling the vapor fence on all four sides, although pre-spill wind tunnel simulations predicted that the cloud would stay within the fence. It was speculated that transport over the top was due to enhanced turbulent mixing from the high spill rate and partly due to superheating of the LNG from the water underneath. This assertion could not be substantiated due to insufficient measurements of concentration and temperature in the source area. A maximum downwind distance to LFL of 330 m (1082 ft) was measured for this case.

Tests were performed with and without the vapor fence. With the fence, the downwind distance to the 2.5% concentration on the ground was reduced from approximately 380 m to 235 m (1246–771 ft) and a substantial reduction in the hazardous areas was also achieved. The persistence of the cloud at a 2.5% concentration near the center of the spill was 530 s with the fence versus 330 s without the fence. Although the fence reduced the downwind distance of the hazardous area and delayed cloud arrival time, it prolonged the cloud persistence time within the fence thereby prolonging the potential for ignition given a source within the reduced area.

For the last test, Falcon-5, a large RPT occurred approximately 60 s after the spill and a fireball started inside the vapor fence at 81 s. This test had a spill rate of 30.3 m^3/min (1070 ft^3/min), total volume of 43.9 m^3 (1550 ft^3), and methane content of 88%. The fireball was speculated to be due to an RPT blowing insulation off of a pipe, which could have had oxygen frozen on its surface due to cooling with liquid nitrogen prior to testing, thereby exposing the natural gas to the oxygen. Only limited data outside the fence was obtained up to a time of about 100 s. RPT's also occurred during Falcon-3 with a spill rate of 18.9 m^3/min (667 ft^3/min), total volume of 50.7 m^3 (1790 ft^3), and methane content of 91%.

3.2. Modeling

Dense gas dispersion models generally fall into the following categories: Navier–Stokes based, Lagrangian non-linear puff, shallow layer or two-dimensional integral, one-dimensional integral, and simplified empirical. The following sections will describe these models and discuss some codes representative of these model types.

3.2.1. Navier–Stokes-based models

The most complex models are those that computationally solve time-averaged, three-dimensional turbulent transport equations that come from conservation of mass, species, momentum, and energy balances. These codes are termed field or computational fluid dynamics (CFD) models and are based upon solving the Navier–Stokes fluid equations. Codes can include the ability to model laminar and turbulent flow fields. Due to computational limitations, not all of the length and time scales associated with turbulence can be simulated. Thus, the conservation equations are averaged such that smaller scales are not resolved. The effects of turbulence at these smaller scales are included by empirically based terms that are added to the averaged conservation equations.

The most well known code for dispersion that is of this model type is FEM3 [58–60] and its subsequent upgraded versions up to FEM3C [61–64]. Developed by Lawrence Livermore National

Laboratory, FEM3 uses a Galerkin finite element scheme in space and a finite difference scheme in time. The latest version, FEM3C, models flow over variable terrain and objects, as well as complex cloud structures such as vortices and bifurcation. Both isothermal and non-isothermal dense gas releases as well as neutrally buoyant vapor emissions can be modeled. It has the capability to model multiple simultaneous sources of instantaneous, continuous, and finite-duration releases. FEM3C also incorporates a phase change model that accounts for water vapor interaction in the cloud, and it has the option to use the *k*-epsilon turbulent transport equations.

Limitations of these codes are in the approximations and assumptions that are used to model turbulence and buoyancy effects. They are the most computationally expensive among the model types, but with the present day computational power, they can be run on a single processor personal computer.

3.2.2. Lagrangian non-linear puff models

Gaussian puff models are typically for buoyant or neutrally buoyant releases such as from an elevated stack source. Recently, the code called second-order closure integrated puff [65] (SCIPUFF), developed by Titan Research and Technology, includes a dense gas release model. SCIPUFF uses a Lagrangian puff dispersion model that models non-linear interaction among a collection of Gaussian puffs to represent a three-dimensional, time-dependent concentration field. Dense gas effects are modeled by using the vorticity form of the momentum conservation equation. Finite duration, unsteady, and multiple sources can be modeled, as well as flow over flat or complex terrain. Comparison to dense gas field data on centerline maximum concentration from Maplin, Burro, and Coyote tests indicated the model under predicts concentration values within a factor of two [62].

3.2.3. Shallow-layer models

Shallow-layer models use equations that assume the lateral dimensions are much greater than the vertical dimension, which is representative of dense gas releases where low wide clouds result. One such model, TWODEE, has been developed for dense gas releases by Hankin and Britter [66,67]. Depth-averaged variables are solved in two dimensions (lateral) using the conservation equations. Empirical correlations are used to determine the entrainment rate of air into the dense plume. The ability to model the effects of complex terrain and phase changes can be incorporated into this model. It is a compromise between Navier–Stokes based models and one-dimensional integral models, though it still requires an order of magnitude greater computational time then one-dimensional integral models.

3.2.4. One-dimensional integral models

One-dimensional integral models such as SLAB [68], HEGADAS [69] and DEGADIS [70] use similarity profiles that assume a specific shape for the crosswind profile of concentration and other properties. The downwind variations of spatially averaged, crosswind values are determined by using the conservation equations in the downwind direction only. The weakness of these models is that they cannot model flow around obstacles or over complex terrain.

The DEGADIS and SLAB models are used widely in the public and private sector due to the convenience of fast computational run time and ease of use. Both can model either buoyancy-dominated, stably stratified, or neutral releases, as well as jet releases. There are some models of this type such as GASTAR, developed by Cambridge Environmental Research Consultants (CERC), that incorporate the effect of terrain such as variable slopes, variable ground roughness, and obstacles including porous obstacles into the integral formulation.

3.2.5. Empirical models

The simplest models are modified Gaussian puff/plume models that are based upon the conservation of species equation. The downwind concentration profiles are represented by ad hoc equations. The cloud is assumed to have a specific Gaussian shape with air entrainment occurring at the cloud edges and the interior of the cloud is assumed to have a uniform composition. Empirical models by Germeles and Drake, Fay and Lewis, Burgess et al., Feldbauer et al., Science Applications, Inc. (SAI), U.S. Federal Power Commission, and U.S. Coast Guard are compared by Havens [71].

3.2.6. Model evaluation studies

Fifteen integral models, including publicly available and proprietary, were evaluated in a validation exercise by Hanna et al. [72] where calculations were compared to data from eight field experiments that included the Maplin Sands, Burro, and Coyote test series. SLAB, HEGADAS, DEGADIS, and GASTAR were able to predict maximum plume centerline concentrations and plume width for these field tests to within a factor of two with a tendency to over predict dispersion distances. It was noted that all of these models were unable to reproduce the variation of concentration with averaging time from field data since they assume that the cloud has a dense gas ‘core’ that is unaffected by averaging time.

Mercer and co-workers [73] compared several integral models against each other, but not to experimental data, by considering 25 cases that varied in wind speed, atmospheric stability, roughness length, spill volume, and pool radius. For each case, the density of the released gas was twice that of air and only instantaneous releases were considered. The model predictions varied within a factor of 3–5, and the greatest differences among the models arose for the case with low wind speed, F-stability class, and large surface roughness length.

An evaluation protocol of dense gas dispersion models has been developed through a program called SMEDIS, a European Union research project funded by the Environment and Climate Research Program [74,75]. The evaluation procedure incorporates validation, verification, and scientific assessment for simple as well as complex situations that include aerosols, topography, and obstacles. Screening tools, integral models, shallow-layer models, and CFD models were compared among a dataset of field and wind tunnel data.

The SMEDIS results show that all models were globally better at predicting arc-wise measurement, such as centerline maximum concentration, than point-wise statistical measures,

suggesting that is more difficult to predict the general cloud shape. The CFD models performed better overall on statistical measures of geometric variance, mean relative square error, and fraction of values within a factor of two for centerline maximum and point-wise concentrations. It was also noted that more information is necessary from field experiments on sensor accuracy and data uncertainty in order to define acceptable agreement with model predictions.

3.2.7. Model directory

The Office of the Federal Coordinator for Meteorology (OFCM) has published a directory of a number of transport and dispersion models for the release of hazardous materials into the atmosphere, including those for cryogenic releases [76]. An in-depth compilation and description of the models are provided as well as model verification and validation information.

4. Combustion events

4.1. LNG pool fire and vapor cloud fire experiments

This section reviews experimental studies of LNG pool fires on water and land, as well as LNG vapor cloud fire studies over water. Table 3 lists the largest tests to date on LNG pool and vapor cloud fires on land and water. These studies have measured radiative heat flux, burn rate, flame geometry, and flame speed. The principal differences found between LNG pool fires on land and water are burn rate and the resulting flame height. Burn rates and flame heights are about a factor of 2 greater on water than on land. The additional heat flux from the water to LNG increases the burn rate and consequently the flame height. Surface emissive power from LNG pool fires on water and land have been found to be similar for equivalent sized pools up to diameters of about 15 m. Comparison between larger diameters isn't possible due to limitations of the largest complete data set for pool fires on water.

Also listed in Table 3 are LNG vapor cloud fire studies, performed in unobstructed and unconfined environments. The vapor cloud fires were found to be non-homogeneous, in which some portions burn as a partially pre-mixed flame and others as a diffusion flame. None of the vapor fire tests have resulted in fireballs, but transient tall flames have occurred principally in the fuel-rich regions. Flame speeds were found to be too low to result in damaging overpressures.

4.1.1. LNG fire experiments over water

4.1.1.1. U.S. Coast Guard China Lake tests [1978]. A series of 16 tests were performed spilling 3–5.7 m^3 (106–201 ft^3) of unconfined LNG onto water with spill rates of 0.02–0.11 m^3/s (0.71–3.9 ft^3/s) at the Naval Weapons Center at China Lake, California [77–80]. The objective of the tests was to measure the thermal radiation output of two types of LNG fires over water; pool fires and vapor cloud fires. Three types of experiments were performed: immediate ignition of the LNG pool, delayed ignition in which ignition occurred after the spill started but before the evaporation was complete, and downwind ignition of the vapor cloud. Of the 16 tests, 7 were pool fire tests, 3 were

Table 3
LNG fire tests on water and land

Study	Spill terrain	Spill volume (m^3)	Spill rate (m^3/min)	Pool diameter (m)	Flame length (m) (*L*/*D*)	Surface emissive power (kW/m^2)		Burn rate 10^{-4} m/s or (kg/m^2 s)[a]	Flame speed for vapor cloud fires (m/s)
						Pool fire	Vapor cloud fire		
U.S.CG China Lake Tests [77–80]	Water	3–5.7	1.2–6.6	~15 (effective)	25–55 (2.8-4.4)	210 ± 20 (narrow) 220 ± 50 (wide)	220 ± 30 (narrow) 200 ± 90 (wide)	4–11 (.18–.495) (calculated)	8–17 (relative to cloud)
Maplin Sands [81–82]	Water	5–20	3.2–5.8	30 (effective)	80 (2.6)	178–248 203 (avg)	137–225 174 (avg)	2.1 (.0945) (calculated)	4.5–6.0
Coyote [84]	Water	14.6–28	13.5–17.1	Not measured	Not measured	Not measured	150–340	Not measured	30–50 (near ignition sources)
Maplin Sands [85]	Land	Not reported	NA	20	43 (2.15)	153 (avg) 219 (max)	NA	2.37 (0.106) (measured)	NA
Montoir [86]	Land	238	NA	35	77 (2.2)	290-320 (narrow angle) 257-273 (wide angle) 350 (max)	NA	3.1 (0.14) (measured)	NA

[a] Some experiments report burn rate and/or mass burn rate in units of m/s and kg/m^2 s, respectively. Conversion between burn rate and mass burn rate was obtained by assuming a density of 450 kg/m^3 for LNG.

delayed ignition tests, and 6 were vapor cloud fire tests. Wind speeds varied from 3.1 to 4.1 m/s (6.9–9.2 mph).

For pool fires, spot surface emissive powers were obtained near the base of the flame indicating a value of $210 \pm 20\,kW/m^2$ ($6.66 \pm 0.63 \times 10^4$ Btu/h ft^2) using narrow angle radiometers, and average emissive power for the entire surface of the flame was $220 \pm 50\,kW/m^2$ ($6.97 \pm 1.6 \times 10^4$ Btu/h ft^2) using wide angle radiometers. Narrow angle measurements correspond to 'spot surface emissive power' values, whereas average surface emissive power measurements use wide angle radiometers and refer to an average over the flame surface and are interpreted based upon a particular geometry for flame area. These values represent averages over all tests. The percentage of methane in the LNG used for each test varied from 75 to 95% however was not controlled as a parameter. The highest spot emissive power of $250\,kW/m^2$ (7.93×10^4 Btu/h ft^2) occurred with the highest concentration of methane.

Average flame heights over the duration of steady burning varied from 25 to 55 m (82–180 ft) and fluctuated ± 10 m (±33 ft) for individual tests. The average flame length to diameter ratios varied from approximately 3 to 4, with a peak value of 6. The pool was not radially symmetric, but was closer to an ellipse with "fingers" emerging from the outer periphery. The dimensions of the "fingers" could not be determined by the motion picture data, thus the pool was approximated as an ellipse. By equating the pool area to that of a circle, the maximum steady-state pool diameter was approximately 15 m (50 ft) for a spill volume of 5.7 m^3 (201 ft^3) and spill rate of 6.6 m^3/min (233 ft^3/min).

The burning rate was estimated by dividing the total volume of LNG spilled by the calculated area of the pool and the duration of intense or steady state burning. The calculated burn rates varied from 4×10^{-4} to 11×10^{-4} m/s ($1.3–3.6 \times 10^{-3}$ ft/s) among all of the tests. It should be noted that the volume spilled during steady state burning was less than the total volume of LNG spilled. By using the total volume of LNG spilled rather than the volume spilled during steady burning, higher burn rates are calculated. If burn rates are calculated based upon the reported values for spill rate and calculated pool area, then burn rates vary from 3×10^{-4} to 9×10^{-4} m/s ($0.98–2.9 \times 10^{-3}$ ft/s). For higher spill rates, it was observed that the burn rates were higher, speculated as possibly due to the interaction between the jet and water effectively increasing the heat transfer area.

For the delayed ignition tests, the pool was ignited approximately 30 s after the beginning of the spill. The vapor cloud burned back to the source to burn as a pool fire. The pool fire portion of the results from these tests was included in the pool fire test data to obtain average values.

For the vapor cloud fires, surface emissive powers were obtained indicating a value of $220 \pm 30\,kW/m^2$ ($6.97 \pm 0.95 \times 10^4$ Btu/h ft^2), using narrow-angle radiometers, and $200 \pm 90\,kW/m^2$ ($6.34 \pm 2.85 \times 10^4$ Btu/h ft^2), using wide-angle radiometers. Vapor cloud fires were observed to propagate along the ground back towards the pool. The flame height to width ratio averaged about 0.5. Flame speed relative to the gas cloud varied from 8 to 17 m/s (18–38 mph). Fireballs were not observed for these spill sizes.

4.1.1.2. Maplin Sands tests [1980]. As described previously in Section 3.1.3, these tests were performed to obtain dispersion and thermal radiation data on 20 spills of 5–20 m^3 (177–706 ft^3) of LNG and 14 spills of 13–31 m^3 (459–1095 ft^3) of propane onto water [81,82]. Wind speed and direction, relative humidity, and radiation measurements taken with 26 wide-angled radiometers were recorded.

Ignition points were placed 90 to 180 m (295–590 ft) downwind of the spill point. Ignition was achieved in 11 out of the 14 tests, 7 LNG and 4 LPG, due to various difficulties. This result could be due to the ignition points placed at cloud peripheries where inhomogeneous and lean burn regions exist. Thus, some ignitions did not result in sustained burns. Radiation and diffusion flame analysis results were reported for 4 LNG tests. Of the four tests reported, 3 were continuous spills with a spill rate range of 3.2–5.8 m^3/min (113–205 ft^3/min), and one instantaneous with a spill volume of 12 m^3 (424 ft^3).

In all of the four LNG tests with ignition, a vapor cloud fire developed, and for one test the vapor cloud fire propagated back to the spill point forming a pool fire. This pool fire lasted only for a few seconds before the fuel was consumed and therefore did not have time to completely develop. As noted by the authors, incomplete photographic records also made the analysis of this test difficult, however an average surface emissive power and burn rate were reported.

An effective pool diameter of 30 m (98 ft) was calculated by approximating the flame base area as an ellipse. The average flame height was 80 m (262 ft). An average surface emissive power of $203\,kW/m^2$ (6.4×10^4 Btu/h ft^2) with a range of 178–248 kW/m^2 ($5.64–7.86 \times 10^4$ Btu/h ft^2) was inferred by using a tilted cylinder solid flame model, and an approximate fuel burn rate of 2.1×10^{-4} m/s (6.9×10^{-4} ft/s) was calculated using the Thomas correlation [83].

It was also found that the flame propagated in the vapor cloud in two modes: as a pre-mixed weakly luminous flame that moved downwind from the ignition point and as a luminous diffusion flame that moved upwind and propagated through the fuel-rich portions of the cloud and burned back gradually to the spill point. Video recordings indicated that pre-mixed burning took place in gaps in the vapor cloud and that the fuel/air concentration was not homogenous. Expansion of the combustion products principally took place vertically.

Diffusion flame propagation speeds of 4.5–6.0 m/s (10–13 mph) moving with the wind were measured. The wind speed range was too narrow to determine possible flame propagation dependency on wind speed. Flame generated overpressures were below 4 kPa (0.06 psi).

In one continuous spill test the pre-mixed flame propagated through the vapor cloud up to 130 m (421 ft) from the spill point. The flame height-to-width ratios of the vapor cloud fires were in the range of 0.2 to 0.4. For vapor cloud fires, an average surface emissive power of $174\,kW/m^2$ (5.52×10^4 Btu/h ft^2) with a range of 137–225 kW/m^2 ($4.34–7.13 \times 10^4$ Btu/h ft^2) was measured.

4.1.1.3. Coyote tests [1981]. The Coyote tests were performed by LLNL and the Naval Weapons Center at China Lake,

California and sponsored by the U.S. DOE and the Gas Research Institute [84]. The burning of vapor clouds from LNG spills on water were studied in order to determine fire spread, flame propagation, and heat flux. Data on 4 spills of 14.6–28 m^3 (516–989 ft^3) with flow rates of 13.5–17.1 m^3/min (44.3–56.1 ft^3/min) were performed with fuel of varying ratios of methane, propane, and ethane. Tests were performed in wind speeds from 4.6 to 9.7 m/s (10–22 mph) and atmospheric stability conditions from unstable to neutral. Gas concentration measurements were averaged over a 2 s period.

The ignition point was located near the cloud centerline about 60–90 m (197–295 ft) downwind of the spill source, and ignition was performed using either a flare or a jet. Ignition took place 100–150 s after the beginning of the spill. The flames were observed to begin near the center of the cloud and propagate radially outward, downwind and upwind toward the spill source. Both visible yellow luminous and transparent flames were observed. Pool fires occurred but measurements were not taken.

Pre-ignition contours were determined by interpolation of 2-s averaged gas sensor measurements. It was found that the pre-ignition 5%-gas-concentration contours are not indicative of the potential burn area and its location. This could be due to the lack of sensors used between the spill point and 140 m (459 ft), and the interpolation scheme used to generate the contours. The actual burn area was observed to propagate further downwind and to the sides than indicated by the pre-ignition concentration contours. The instantaneous 5% gas concentration contours closely coincided with the burn region at sensor locations when 2 s averaging of concentration measurements were used rather than a 10-s averaging.

In the test with the highest flow rate or total volume spilled, 17.1 m^3/min or 28 m^3 (604 ft^3/min or 989 ft^3), RPTs increased the distance to the downwind LFL by about 65% and the total burn area by about 200%. The flame extended up to 280 m (918 ft) downwind and had a maximum width of 60 m (197 ft). The authors note that the increase was caused by an increased source rate and by enrichment in higher hydrocarbons. The puffs of vapor from the RPTs cause momentary increases in concentration as they propagate downwind.

The test conducted in the lowest wind speed and most stable atmospheric conditions had the broadest vapor fire cloud with a maximum width of 130 m (426 ft) and downwind distance of 210 m (689 ft).

Flame heights appeared to vary directly with the pre-ignition height of the combustible mixture near the ignition source. The ratio of flame height to cloud height varied from 5 to 10. The clouds were 3–8 m (9.8–26 ft) in height. Flame speeds with peak values of 30 m/s (98 ft/s) were observed near weak ignition sources and 40–50 m/s (131–164 ft/s) for strong ignition sources. Speed decreased as a function of distance from the source and no flame acceleration was observed. Overpressures of only a few millibars were measured.

Heat flux (radiative and convective) measurements inside the vapor cloud fires were found to be in the range of 150–340 kW/m^2 (4.76–10.8 $\times 10^4$ Btu/h ft^2). External radiative flux values for the bright yellow portion of the flames were in the range of 220–280 kW/m^2 (6.97–8.88 $\times 10^4$ Btu/h ft^2) using wide and narrow-angle radiometers. The external radiative flux measurements were noted as being suspect because the sensors were not protected by a heat sink or water-cooling. This lack of cooling resulted in the sensors heating up and the signal becoming distorted as the heat load increased.

4.1.2. LNG fire experiments over land

4.1.2.1. Maplin Sands tests [1982]. Tests sponsored by Shell were performed to measure the thermal radiation from 20 m (66 ft) diameter contained land-based pool fires of LNG, LPG and kerosene using both wide and narrow-angle radiometers [85]. The following were also measured: mass burning rate, fuel composition, wind speed and direction, relative humidity, and metal surface temperatures close to the fire. Video and still photographs were taken upwind and crosswind of the fires. One test was performed for each fuel.

For the LNG fire, the flame appeared roughly cylindrical in shape and tilted due to a 6.15 m/s (13.8 mph) wind. The measured burning rate was 0.106 kg/m^2 s (0.0217 lb/ft^2 s)) for LNG, versus 0.13 kg/m^2 s (0.0266 lb/ft^2 s) for LPG. The production of black soot appeared at a much higher elevation in the flame and was significantly less than that produced by LPG or kerosene. The measured mean flame length using video recordings for the LNG fire was 43 m (141 ft) with a flame length-to-diameter ratio of 2.15. The Thomas correlation for flame length-to-diameter ratio predicts a value of 1.88 if the measured burning rate is used, underestimating the observed mean flame length by 12.6%.

The average surface emissive power was inferred by measurements made using wide-angle radiometers and the use of a solid flame model and the Thomas correlation representing the flame as a tilted cylinder. The average surface emissive power determined for the LNG pool fire was 153 kW/m^2 (4.85 $\times 10^4$ Btu/h ft^2), while LPG had a much lower value of 48 kW/m^2 (1.52 $\times 10^4$ Btu/h ft^2) due to the greater smoke shielding. The maximum measured value using narrow-angles radiometers for the LNG fire included values up to 219 kW/m^2 (6.94 $\times 10^4$ Btu/h ft^2).

4.1.2.2. Montoir tests [1989]. These tests were a collaboration among many sponsoring companies: British Gas, British Petroleum, Shell, Elf Aquitaine, Total CFP, and Gaz de France with tests performed by British Gas, Midlands Research Station, Shell, and Thornton Research Center [86]. Tests on 35 m diameter LNG pool fires on land were performed at a facility near the Montoir de Bretagne methane terminal.

A total of three LNG pool fire experiments over a wind speed range of 2.7–10.1 m/s (6.0–22.6 mph) were performed. The maximum volume of LNG poured into the 35 m (115 ft) diameter bund was 238 m^3 (8405 ft^3). The following were measured: flame geometry, incident thermal radiation at various ground level positions, spot and average flame surface emissivity, gas composition in pool, fuel mass burning rate, and flame emission spectra in both the visible and infra-red regions.

Small regions of the flame were examined using a narrow angle radiometer. Two types of average surface emissive powers were employed: one based upon heat flux measurements and an

idealized cylindrical flame shape that includes the smoky part of the flame, and the other based from cine photographs that represent the actual areas of flame unshielded by smoke.

A mass burn rate for a methane fire was obtained as long as the vapors above the pool were measured to have at least a 99-mol% methane content. During the methane pool fire burn time, the ethane content in the vapors above the pool was less 0.2-mol% in order to avoid the high smoke production that can occur from ethane, as well as the decrease in the mass burn rate from the increased conduction into the fuel due to higher boiling point of ethane.

All fire tests were observed to have intensely bright regions extending from the base to at least half of the total flame height, and the rest was obscured intermittently by smoke. Smoke yield was greater than that produced in a 20 m (66 ft) diameter LNG fire. The shape of the fire was observed to be complex and was noted as difficult to represent using simple geometries.

The average mass burning rate among the all tests was 0.14 kg/m^2 s (0.029 lb/ft^2 s). Flame drag ratios up to 1.29 for high wind speeds, and 1.05 for low wind speeds were measured. Flame drag ratio is defined as the flame base length in the direction of the wind divided by the pool diameter. The time averaged maximum flame height to pool diameter ratio was approximately 2.2.

At 140 m (459 ft) from the bund center, the incident thermal flux was measured as approximately 15 kW/m^2 (4.76×10^3 Btu/h ft^2) downwind, 5 kW/m^2 (1.59×10^3 Btu/h ft^2) crosswind, and 3 kW/m^2 (0.951×10^3 Btu/h ft^2) upwind during a wind speed range of 7.0–10.1 m/s (16–22.6 mph).

In the lower 10 m (33 ft) of the flame, typical time averaged spot surface emissive powers of 290–320 kW/m^2 ($9.19–10.1 \times 10^4$ Btu/h ft^2) were measured in the crosswind direction. Values up to 350 kW/m^2 (11.1×10^4 Btu/h ft^2) averaged over 5–10 s periods were measured. These values are much greater than measured for smaller pool fires where, at comparable positions, values of 140–180 kW/m^2 ($4.44–5.71 \times 10^4$ Btu/h ft^2) for a 6.1 m (20 ft) diameter fire and 170–260 kW/m^2 ($5.39–8.24 \times 10^4$ Btu/h ft^2) for a 10.6 m (35 ft) diameter fire have been observed.

For all tests, the range of time averaged surface emissive power values for individual wide-angle radiometers was 230–305 kW/m^2 ($7.29–9.67 \times 10^4$ Btu/h ft^2). Values averaged among all instruments for each experiment were in the range of 257–273 kW/m^2 ($8.15–8.65 \times 10^4$ Btu/h ft^2). The instantaneous readings from these instruments were used to obtain an average surface emissive power over the surface of the flame by deriving view factors from video cameras.

Values of surface emissive power were also obtained by utilizing incident flux data and an idealized flame shape based upon a tilted cylinder with length calculated from the Thomas equation [83] and tilt angle from the Welker and Sleipcevich [87] equation. The values calculated were much lower with a range of 130–180 kW/m^2 ($4.12–5.71 \times 10^4$ Btu/h ft^2). With both methods, the average surface emissive power was plotted for pool diameters of 6.1, 10.6, 20, and 35 m (20, 35, 66, 115 ft). The graph indicated that the rate of increase of the average surface emissive power for increasing pool diameter decreases with increasing diameter. The authors [86] speculate that it is not expected that a much greater value would be obtained for larger pool fires.

4.2. Deflagration/detonation experiments

Explosions from combustion of flammable fuel–air mixtures are classified as either a detonation or deflagration. In a deflagration, the mixture burns relatively slowly, on the order of 1 m/s (3 ft/s) for hydrocarbon–air mixtures, though speeds will greatly exceed this if the flame is accelerated due to flow interaction with obstacles. This flame speed is in contrast to a detonation where the flame front travels as a shock wave followed closely by a combustion wave, which releases energy that sustains the shock wave. The detonation velocity for hydrocarbon–air mixtures is on the order of 2000–3000 m/s (6000–10,000 ft/s). Consequently, detonations generate very high overpressures, and hence are more damaging than deflagrations. Deflagrations can produce overpressures up to around 0.8 MPa (115 psi), while detonations produce overpressures up to around 2.0 MPa (300 psi). Additional hazards from explosions are fragments resulting from damaged structures. Modeling and experimental studies of projectile hazards resulting from explosion is reviewed by Davies [88]. The amount of explosion overpressure is determined by flame speed, which is a function of the turbulence created within the vapor cloud and the amount of vapor within the flammability limits. In order for a vapor cloud explosion to occur, the LNG vapor must be sufficiently mixed with air to form a mixture within the flammability limits.

The type of explosion that occurs depends upon the strength and geometry of the ignition source, the reactivity of the fuel, the degree of confinement, and the obstacle density. Fuel reactivity is classified as low, medium, and high, and is a qualitative measure of a fuel's capacity to accelerate to high flame speeds. Increasing reactivity corresponds to increasing capacity to accelerate flames. A deflagration may transition to a detonation when there is a high degree of confinement or blockage such as with closely spaced obstacles. The obstacles will create turbulence which enhances the burning surface area and increases the local burning velocity. Detonations are more easily achieved with high reactivity fuels, high energy ignition sources, and a high degree of confinement.

Detonation of pure methane–air mixtures is very difficult since methane is a low reactivity fuel, but with the addition of higher reactivity fuels the difficulty decreases. LNG is composed principally of methane (85–95%), but may contain ethane up to 15%, and propane up to 5%, depending upon the source. The addition of small amounts of ethane and/or propane (10%) can reduce the required ignition charge for detonation by almost a factor of 10. Differential boil-off from an LNG pool can cause the vapor cloud to have a different composition than the liquid, and to have varying composition within the cloud. Initially, the vapors that evolve will be mostly methane and the heavier hydrocarbons will boil off last. Thus, there may be portions of the cloud rich in the heavier hydrocarbons that occur later in the spill. However, due to limited mixing, the entire vapor cloud will not have a composition within the explosion limits of the

constituent fuels of LNG in air. Deflagrations are the more probable mode of combustion in accident situations since detonations are very difficult to achieve.

There have been several reviews on explosions of hydrocarbon–air mixtures [89–91]. It was pointed out by Moen [90] that weak ignition of vapor clouds in an unconfined and unobstructed environment is highly unlikely to result in a deflagration to detonation (DDT) even for more sensitive fuel–air mixtures, but is more likely with confinement and the presence of obstacles. Nettleton [91] indicates that the understanding of how confinement, temperature, pressure, and mixture composition influence the initiation source and distance to DDT is not complete, and that further work must be done before prediction can be made whether DDT will occur for any given spill scenario.

The following is not intended to be an extensive review, but is intended to bring out some of the important aspects regarding explosive properties of methane mixtures.

4.2.1. Bull and Martin [1977]

These experiments studied spherical detonation of methane–oxygen mixtures diluted with nitrogen [92,93]. Detonation of the mixture, contained in polythene bags of uninflated sizes of 1.8 × 1.8 m (5.9 × 5.9 ft) and 3.05 × 1.52 m (10 × 5 ft), was initiated by electrically firing Tetryl explosive. Based upon extrapolation of results for five different charge masses up to 520 g (1.14 lb) it was indicated that more than 20 kg (44 lb) of Tetryl would be necessary to initiate a spherical detonation in a stoichiometric mixture of methane–air, and that a path length of 11 m (36 ft) would be required to experimentally verify the extrapolation. This extrapolation to 20 kg (44 lb) of Tetryl had 95% confidence limits of 8.3–59.7 kg (18–131 lb).

It was also found that the amount of Tetryl required to initiate detonation for methane is more than two orders of magnitude greater than that for most other hydrocarbons, though if heavier hydrocarbons are added, such as ethane, the amount of explosive required will greatly decrease. An extrapolation to a methane–ethane mixture of 90–10 indicated that the required charge strength would decrease to 3 kg (6.6 lb), as compared to 20 kg (44 lb) for pure methane.

4.2.2. U.S. Coast Guard China Lake tests [1978]

Tests were performed in a detonation tube and 5 m (16 ft) and 10 m (33 ft) radius hemispheres [94,95]. Both explosively initiated and spark-ignited tests were performed on methane–air and methane–propane mixtures. For the detonation tube experiments, the methane–air mixture did not detonate using a 5 g (.011 lb) or 90 g (0.21 lb) booster, nor did it detonate with spark ignition. Methane–air mixtures did not detonate with explosive charges up to 37 kg (81 lb) for the 10 m (33 ft) diameter hemisphere tests. Methane–propane mixtures of 60–40, 70–30, and 85–15 did detonate using a 1 kg (2.2 lb) high explosive booster for the 5 m (16 ft) hemisphere tests.

Experiments were also performed to test a postulated accident scenario in which the vapor formed during an LNG spill mixes with air to form a flammable mixture and then diffuses into a culvert system. The mixture in the culvert ignites and the combustion wave accelerates to transition to a detonation which exits the culvert and then potentially detonates the remaining unconfined vapor cloud. The detonation charge used in the culvert was a 13 kg (29 lb) explosive. Detonations only occurred when methane was mixed with propane concentrations 6% or greater and the culvert measured 2.4 m (7.9 ft) in diameter.

4.2.3. Vander Molen and Nicholls [1979]

Experiments were performed to measure the effect of ethane addition to methane air clouds on detonation [96]. A stoichiometric mixture with air was maintained for every mixture of methane and ethane tested. The ethane concentration ranged between 0 and 5.66% by volume of the total methane–ethane–air mixture. The experiments were performed using a sectored shock tube of 147.6 cm (4.84 ft) radius and 5 cm (0.16 ft) width to model a 20° pie shaped sector of a cylindrical cloud. For an ethane content of 1% by volume in the methane–ethane–air mixture, or a 10% ethane by volume content in the fuel, 5.5 g (0.012 lb) of condensed explosive or critical initiating blast energy of 25,000 J/cm was needed to result in a detonation.

4.2.4. Moen et al. [1980]

Work was performed at McGill University in Montreal, Canada on flame acceleration and deflagration to detonation transitions [97]. The influence of obstacles on flame acceleration of methane–air mixtures was investigated in a cylindrical vessel 30.5 cm (1 ft) in radius. The effect of obstacles was to increase flame speed of up to 130 m/s (426 ft/s), 24 times the velocity without obstacles. The high flame speeds could only be maintained with repeated obstacles, which provide large-scale flow field distortions associated with flame acceleration.

4.2.5. Harrison and Eyre [1987]

A series of tests were performed to investigate the effect of obstacle arrays on flame acceleration of premixed natural gas–air and propane–air mixtures [98]. A wedge-shaped enclosure was used which had an open top and bounding sidewalls forming a 30° wedge of 30 m (98 ft) long and 10 m (33 ft) high. This aspect ratio was used so that a shape representative of a dense cloud would be modeled.

A series of horizontal pipes were placed in the wedge to provide optimal flame acceleration. Blockage ratios of 20 and 40%, based upon the percentage of the obstacle grid, were used. Unobstructed and obstructed tests were performed using a low energy fusehead igniter. The effect of grid height, blockage ratio, grid spacing, and the total number of grids were investigated. Unobstructed natural gas–air mixtures produced low flame speeds of 8–9 m/s (26–30 ft/s) in the first few meters and overpressures of 4–5 mbars, which decayed with a $1/r$ relationship in the far field.

Grids with low blockage ratios or low height produced overpressures not sufficient to cause severe structural damage of 29–63 mbars decaying as $1/r$ and flames speeds of 37–51 m/s (121–167 ft/s). The test with the highest obstruction obtained a maximum flame speed of 119 m/s (390 ft/s) (±20%) and overpressure of 208 mbars decaying as $1/r$, which can be sufficient to cause structural damage to buildings in the immediate vicinity of the cloud. In all tests, flame speed and overpressures decayed

rapidly after the flame emerged from the grid of obstacles, typically within 5 m (16 ft) of the last grid. Thus, the size of the obstacle array, not the size of the gas cloud, defined the size of the pressure source.

4.2.6. Shell [2001]

Flame acceleration was investigated in a vented box structure, 10 m (33 ft) long, 8.75 m (29 ft) wide, and 6.25 m (21 ft) high using methane–air and propane–air mixtures ignited using a conventional spark plug [99]. Results indicate that an initially stable and subsequently unstable flame propagation regime occurs. In the unstable regime, instabilities grow to wrinkle the flame and increase the flame speed. Flame speed measurements up to a radius of approximately 3 m (10 ft) indicate that flame speed increases with radial distance and varies as the square root of time. Cell size was measured photographically as the flame progressed through the box. The cell size ranged from 200 to 400 mm (7.87–15.7 in.), which is typically 4 times the size of ethane or propane under stoichiometric conditions [100], indicating the lower sensitivity of methane to detonation.

4.3. Fire modeling

Generally, three approaches can be identified to modeling thermal radiation from pool fires. These models are classified as point source, solid flame, and field. Schneider [101] provides a review of the first two models and various vapor cloud and fireball models pertaining to LNG.

The simplest model is the point source model where the emission of thermal radiation is treated in a global manner by assuming the radiation source is a point and that the radiation decays as the inverse square of the distance from the source. An empirical fraction of the heat of combustion is used to approximate the thermal radiation emitted, the uncertainty of which increases with large pool fires due to the lack of comprehensive heat flux data. It is also assumed that the receiving surfaces are oriented to receive the maximum thermal radiation.

The heat flux in the near field, approximately within two pool diameters, is not predicted adequately with this model because the geometric considerations between the emitting flame and receiving surfaces become important. The effect of flame tilt from wind and the presence of objects interacting with the flame cannot be modeled using the point source approach.

The next level of increasing complexity is the solid flame model, which models the surface of the flame with a simple, usually cylindrical, geometry [102–105]. The thermal radiation is uniformly emitted from this surface and the average radiant surface emissive power is based upon empirical correlations with pool diameter. For an assumed geometry, the geometric view factor, which is the fraction of radiant energy that is received by an object's field of view can be determined exactly [106]. The attenuation of the thermal radiation by water vapor and carbon dioxide in the atmosphere can be represented in the model.

In order to capture the tilting of the flame due to wind, a tilted cylindrical flame shape is typically used. Flame length, tilt and drag necessary to determine flame shape and view factors are based upon empirical correlations. For pool fires with simple pool geometries, and where parameters are well known, these models provide good agreement with experiment. Johnson [105] found agreement within one standard deviation from the average measured heat flux from radiometers for a range of pool sizes, 1.8–35 m (5.9–116 ft) in diameter. The disadvantage of these models is the inability to model more complex flame shapes such as those arising from irregular shaped pools or object interaction with the flame zone.

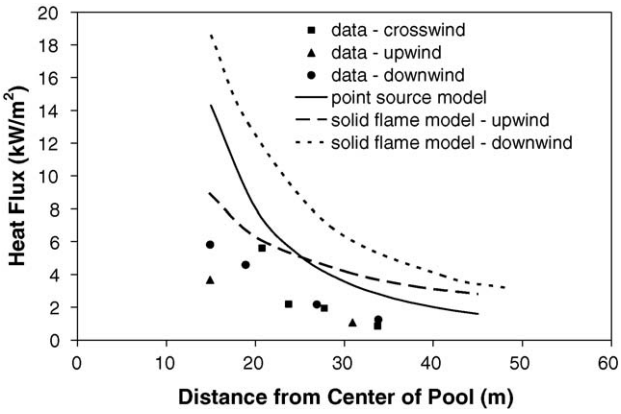

Fig. 3. Point source and solid flame model comparison to trench fire data in crosswind.

Shown in Fig. 3 is a comparison of these models to trench fire data obtained by Croce et al. [107] with trench dimensions of 23.5 m × 1.83 m (77 × 6 ft). The pool was far from circular, but for this demonstration the pool is assumed to be a circle for the solid flame model. For the point source model the flame is assumed to radiate from the center point, thus the pool shape is irrelevant for this model. The measured wind speed was 1.83 m/s (4 mph), average flame length 3.4 m (11 ft), flame tilt 56.8°, flame drag ratio 2.96, burning rate .054 kg/m^2 s (0.011 lb/ft^2 s), and average surface emissivity 135 kW/m^2 (4.28×10^4 Btu/h ft^2). The radiative fraction used for the point source calculation was 0.348 based upon a relation by Moorhouse and Pritchard [108] for radiative fraction as a function of surface emissive power and flame height to diameter ratio. The effective pool diameter is 7.4 m (24 ft) for the given trench dimensions. Thus, the surface emissive power and flame height to diameter ratio was taken into account through the radiative fraction value. The flame height to diameter ratio of 1.49 was calculated using a correlation by Moorhouse [109] that includes the effect of wind. The view factor for a tilted cylinder to an object was calculated by formula derived by Sparrow [110].

The measured burn rate value from experiment was also used for the point source calculation. Fig. 3 indicates that both models over predict the measured heat flux at various distances at crosswind, upwind, and downwind locations. The point source model for downwind values provides the best agreement to experiment about five pool diameters from the pool center. The percent difference between experiment and the point source model results for heat flux measurements downwind range from 4 to 30%, crosswind from 30 to 230%, and upwind from 220 to 290%.

The solid flame model predicts much higher heat flux values since the predicted flame height for the assumed circular pool is much higher than the experimental value, 11 m versus 3.4 m (36 ft versus 11 ft). The discrepancy is principally attributable to flame break up due to the large aspect ratio of the fire. The experiments showed the flame breaking up into flamelets or individual fire plumes. Thus, the flame height is shorter than that of a circular pool fire with equivalent area. The solid flame model can be applied to trench fires as demonstrated by Croce et al. [107], with results for this case within experimental uncertainty ($\pm$0.14–0.51 kW/m^2), but the pool shape must be known a priori. For situations that can result in an irregular shaped pool that isn't known a priori a CFD code must be used for thermal hazard prediction.

The most sophisticated models solve the Navier–Stokes equations that govern fluid flow. These models are also termed field models or computational fluid dynamics-based codes. Since pool fires are turbulent for the scale of interest, turbulence models, typically the *k*-epsilon model, are used. Combustion models typically assume that combustion is mixing-controlled, rather than controlled by the chemical reaction time. The radiative transport equation, along with simplifying assumptions, is used to model thermal radiation. Soot models are also incorporated which invoke empirical models.

The disadvantage of field models is the computational requirements compared to solid flame models, though with the emergence of more powerful computers this issue is less problematic. These codes can now be run on personal computers and workstations, instead of super computers. The advantage of field models is that complex flame shapes can be captured such as those arising from object/flame interaction as from an LNG ship and a pool fire. Vapor cloud fires and fireballs can also be modeled with these codes. Various field models are available such as FLACS, CFX, Phoenics, Kameleon, and Vulcan. These codes vary in their capability to model explosion, fireballs, vapor cloud fires, and/or pool fires.

Although field models invoke a more comprehensive set of physics than simpler, more empirically based models, they will perform poorly if they do not include physics applicable to the problem. The simpler models may perform better in this case. Thus, it is important to develop applicable models and to compare simulation results to experimental data. Models should be extensively validated before they are used for hazard prediction. Discussion and guidelines for validation requirements are provided by Gritzo et al. [111].

5. Discussion and recommendations

Although much information has been obtained from the tests to date, there are remaining technical gaps related to understanding the dynamics and subsequent hazards of a large LNG spill on water. For a hazard analysis it would be ideal to have data on all the pertinent parameters from full-scale tests. It is evident, due to the scale involved in many hazards considered, that it is not feasible to perform such tests, thus data must be obtained from tests on a smaller scale. Models can be developed and validated from the smaller scale data to predict behavior at full scale provided no significant thresholds or differences in phenomena occur. Models should therefore be validated to reflect the physical processes at the larger scale.

The possible spill volume from a single ship's tank is on the order of 10,000 m^3 (35×10^4 ft^3), and the largest experimental spill volume tested to date is 193 m^3 (6.82×10^3 ft^3). Thus, the available experimental results are 2–3 orders of magnitude less than the scales of interest. Although tests the size of a ship tank are likely cost prohibitive, there are gaps in our knowledge base required for hazard prediction that can be addressed at feasible test scales. These will be discussed in Sections 5.1–5.3.

5.1. Factors affecting pool area

A recent analytical study by Cornwall and Johnson [4–5] indicated that waves could have a significant effect on pool diameter. In this model, the effect of waves is incorporated through a conditional statement at the boundary of the pool; namely, the pool will stop spreading once the LNG pool thickness drops below 60% of the wave height. The model assumes cycloid-shaped standing waves, which results in a 27% increase in surface area over a flat surface, thereby increasing the evaporation. The inclusion of this model significantly reduced the pool radius from 253 m (830 ft) to 55 m (180 ft). Thus, it is important to determine by experiment the extent that waves effect spreading.

If the waves are thought of as having a simple cycloid shape and a limiter is imposed on spreading as Cornwall assumed in his model then it could be argued that the area of LNG in contact with the water would not significantly change. It's equivalent to transforming a 2D membrane into a 3D surface while maintaining the surface area, but decreasing the perimeter.

But, this simplistic view of a wave is misleading. In reality, waves are much more dynamic. The ocean or sea surface is not smooth, but rather is turbulent with vortex structures which provide mixing. For a given volume of fluid, the surface area of LNG in contact with water would increase if the LNG is stretched, or its thickness decreased, and/or if contact above and below the LNG occurs as would be the case if the LNG were entrained into a vortex structure.

Currents associated with waves, which could transport the waves further away from the spill than in a calm condition, can play a significant role. It would also be more likely that waves would cause the pool to break up much sooner than a quiescent surface. Determining the spreading and vaporization of the LNG pool is instrumental in determining the evolution of the vapor cloud and subsequent related hazards. If this component is done incorrectly, the rest of the analysis if severely affected.

Currently, there is no experimental data on the effect of waves and currents on pool spreading. It would be valuable to perform a series of relatively small-scale tests in a controlled wave environment to determine the effect of wave parameters on spreading. As mentioned previously in Section 2.3, measurements of pool spread have typically been done by using overhead photography. This technique has the difficulty that LNG vapors block the

liquid pool. Underwater visuals of the spreading pool may also be beneficial.

Measuring the burn rate for LNG fires in such conditions would also be valuable. Since there are cost and feasibility limitations of testing, computational fluid dynamic codes, once validated, could be utilized to investigate an extended parameter space. This effect would require the development of a model of LNG spreading over a wave surface and validation with the experimental data.

Another area where computational fluid dynamic models are of potential utility is the dynamics of the LNG spilling from a breach in a tank. It would be beneficial to experimentally and computationally analyze above and below waterline releases in order to determine the rate and amount of LNG spilled onto the water for complex hole configurations.

5.2. Dispersion

The experimental data on the behavior of an LNG vapor cloud to date is quite extensive, particularly the large-scale work preformed by Lawrence Livermore National Laboratories as shown in Table 2. The findings indicate that the extent of the cloud can be affected by several factors which include wind speed, atmospheric stability, spill rate, method of release (under versus above water), rapid phase transitions, obstructions, and terrain. Low wind speeds and stable atmospheric conditions result in the greatest distance to LFL. Underwater release results in a more buoyant cloud than an above water release. Larger spill rates and rapid phase transitions increase the distance to LFL, while obstructions and rough terrain decrease the distance.

The largest spill in which concentration measurements were taken without the presence of a vapor fence was the Burro series, with a maximum spill volume of almost 40 m^3 (1.41×10^3 ft^3). Whether the spill sizes investigated to date give an indication of the atmospheric dispersion that would occur for spills on the order of 10,000 m^3 (35×10^4 ft^3) is unknown. It can be speculated that dispersion behavior similar to Burro 8 would occur. The Burro 8 test results as discussed in Section 3.1.4 show that the cloud does not dissipate as quickly due to the lack of turbulent mixing and thus will persist for a longer time for low wind speeds and stable atmospheric conditions. This result has hazard implications that may be more pronounced, even in the presence of higher wind speeds and less stable conditions, for very large spills in which the total mass of the dense cloud will be greater.

Though there has been much data obtained on dispersion, performing tests with intermediate spill volumes would be beneficial since it would bring the state of knowledge another order of magnitude closer to the scale of interest. Having data with sensor accuracy and uncertainty reported for a spill volume around 200 m^3, feasible with existing facilities, would provide additional data for model validation. Since a large extrapolation to the scale of interest is still required, modeling efforts should employ field models because they provide a more complete incorporation of the fundamental fluid dynamical equations than other models and have shown to perform better on validation comparisons as discussed in Section 3.2.6.

5.3. Fire

There have been several LNG fire studies of pool and vapor cloud fires on land and water to determine thermal radiation, burn rate, and flame speed. Table 3 specifies spill conditions and measured surface emissive power, burn rate, and flame speed for LNG fire experiments for the largest spills to date. It is evident that there is a lack of data for large LNG pool fires on water. The most complete data set to date for a LNG pool fire on water is from a pool approximately 15 m (50 ft) in diameter and spill volume of 5.7 m^3 (201 ft^3) performed by the U.S. Coast Guard [77–80]. The experiments at Maplin Sands [81–82] involved a larger test with an effective pool diameter of 30 m (98 ft), but as noted, the fire did not have time to fully develop. It was also noted that photographic records necessary for comprehensive analysis were incomplete.

Thus, it would be highly valuable to perform well-instrumented experiments of LNG pool fires on water with pool diameters that extends the current data set on burn rate, flame height, surface emissive power, smoke production, as well as spectral emission characteristics, necessary for the determination of the atmospheric absorption of the LNG thermal radiation. It can be shown that predicted thermal hazard distances can vary by a factor of 2–3 using the solid flame model for a pool fire and the range of values for burn rate and surface emissive power listed in Table 3. Obtaining further data will significantly reduce this uncertainty. Most importantly in such tests, parameters should be well controlled. In the tests performed by the U.S. Coast Guard [77–80] three controlling parameters for burn rate were allowed to vary simultaneously, namely spill rate, LNG composition, and wind speed. Thus, it is not possible to determine the individual contribution of these parameters, as well as their influence on the interpretation of the results.

The surface emissive power has been shown to initially increase with increasing pool diameter as indicated by the Montoir experiments [86] on land for pool fires up to 35 m (115 ft). There was indication of the existence of a maximum value for surface emissive power when plotted as a function of pool diameter. The limit appeared to be reached near a pool diameter of 35 m (115 ft), and thus the surface emissive power would not be expected to significantly increase for larger diameters. After attaining a maximum value, the surface emissive power would expect to decrease with further increases in diameter due to smoke covering the exterior. Although, smoke is made up of a mixture of gases, vapors, and particulate matter from a fire, carbon particulates, or soot, is the particulate matter of smoke and is responsible for the luminosity of the fire. Cold soot in the smoke will absorb a significant portion of the radiation to result is much lower emission to the surroundings. In the Montoir experiments [86], smoke shielding was observed in the upper half of the 35 m (115 ft) diameter LNG fire, while the lower half was highly emissive and smoke free. This behavior is observed with heavier hydrocarbon fuels, but with smoke shielding at smaller diameters and occurring much closer to the fuel surface in an equivalent sized fire.

It has been found for heavier hydrocarbons the surface emissive power asymptotes to a value of about

40 kW/m^2 (1.3×10^4 Btu/h ft^2) [112]. This is a time-averaged, area-weighted value based on portions of the flame covered by black smoke with an emissive power of approximately 20 kW/m^2 (6.3×10^3 Btu/h ft^2) [112], and flame zone regions having higher surface emissive powers which periodically breaking through the smoke. Thus, it would be expected that LNG, at some pool diameter, would display similar behavior, but the diameter at which this occurs is unknown due to lack of data at very large scales. Analytical studies to date have used a surface emissive power of around 200 kW/m^2 (6.3×10^4 Btu/h ft^2) from available data to determine thermal hazard distances. With smoke shielding, this value would significantly be reduced for larger fires, and hence reduce the thermal hazard distances.

Furthermore, pool fire characteristics such as mass fire behavior can change as the pool diameter increases. Several researchers have theorized that there is a pool diameter limit at which the flame envelope breaks up into multiple fires or flamelets, defined as a mass fire. The heights of these flamelets are much less than the fuel bed diameter [113–118].

The view factor, used to determine how much radiative flux an object receives, is very sensitive to flame height at distances greater than about one pool diameter from the fire. The view factor is a function of flame height and is greater when the field of view of the fire is greater for a target, that is, it comprises a greater portion of the total field of view to a surface. This results in a greater amount of heat flux received. When close to a fire, the fire fills the field of view and the view factor approaches unity. Thus, if a mass fire does in fact occur, the amount of heat flux received by an object greater than about a pool diameter away would be less than that of single coherent plume assumption, thereby decreasing the thermal hazard distance.

There is also great uncertainty in flame height at large pool diameters for coherent fire plumes. Several flame height correlations based upon pool fires much smaller ($\leq$30 m [100 ft]) than those presently considered have been developed [83,113,115–121]. Flame height to pool diameter ratios (L/D) for LNG can vary by a factor of 2–3 among these correlations for a given pool diameter. The variation among the correlations may be due to differences in the pool geometry tested, as well as differences in the measurement technique and definition of flame height.

Flame height correlations are typically expressed in terms of a non-dimensional heat release rate, $Q^* = Q/\rho_a T_a C_p g^{1/2} D^{5/2}$, where $Q = \dot{m}\ \Delta H$ is the theoretical heat release rate based upon the fuel flow rate and the heat of combustion, ΔH, and D is the characteristic pool dimension of the fire. The density, ρ_a, temperature, T_a, and the specific heat at constant pressure, C_p, are evaluated for air at atmospheric conditions. This non-dimensional parameter can be experimentally varied by either varying the fuel flow rate or the pool diameter. Thus, very low Q^* can be achieved by either lowering the fuel flow rate or increasing the pool diameter. Due to the experimental difficulties associated with very large-scale tests, it is preferable to lower the fuel flow rate within a representative range of pool diameters.

Heskestad [118], based upon experiments involving fires on horizontal 7.3 m × 7.3 m (24 ft × 24 ft) wood-fiber boards having a very low burn rate, developed a correlation predicting the pool diameter at which break up occurs. Using his results, he predicted L/D would be zero, the limit for mass fire behavior, at a pool diameter of 8900 m for an LNG pool fire [116]. He used a mass burn rate of 0.1 kg/m^2 s (0.02 lb/ft^2 s) for this calculation.

Using the range of mass burn rates 0.0945–0.495 kg/m^2 s (0.019–0.101 lb/ft^2 s) taken from experimental data listed in Table 3 for LNG pool fires on water and Heskestad's correlation, the range of predicted diameter values for which L/D is zero is 7800–215,000 m (5–130 mi.). A nominal value for burn rate of 0.23 kg/m^2 s (0.047 lb/ft^2 s) would result in a break up diameter of 45,000 m (28 mi.). The applicability of this correlation to predict the break-up of LNG pool fires is questionable in light of such large distances and would indicate that further investigation is warranted.

In order for a dimensionless parameter to apply over many length scales, the flow field must exhibit dynamic similarity. The flow dynamics of pool fires is a strong, not exclusive, function of pool diameter. For pool fire diameters less than 10 cm (0.3 ft) the flow field of the visible flame is considered laminar, and for diameters between 10 cm (0.3 ft) and 1 m (3 ft) the flow is in transition to turbulence, and for diameters above 1 m the flow becomes fully turbulent. The pool-like gas burner experiments to date have not been in the fully turbulent regime. The experiments performed by Heskestad have been the only tests performed that have been in the turbulent regime and have investigated a value of Q^* low enough to display break-up behavior, but only with wood-fiber boards. It would be beneficial to perform tests for additional fuels.

As previously noted, low values of the dimensionless parameter, Q^* correspond to large pool diameters. Low values of Q^* can be achieved by lowering the fuel flow rate issuing from the pool surface, rather than the alternative of testing at full scale. Previous researchers have taken this approach by using pool-like gas burners in which the mass flux of fuel issuing from the pool surface can be controlled. Small values of Q^* have been studied, but with small pool diameters (<0.5 m (1.6 ft), Zukoski et al. [119]) (<0.6 m (2 ft) square, Cox and Chitty [115]) (<.0.0046 m (0.015 ft), Becker and Liang [120]) and low mass flux values. All of these researchers have demonstrated that break-up occurs for sufficiently low values of Q^*. The value of Q^* for which break-up occurs has not been conclusive due to differences in pool geometry and the scale at which the tests were performed.

Further experimental testing under conditions of low values of Q^* and flow dynamic similarity would be valuable with pool-like gas burners at scales of fully turbulent fires. This could be achieved with a gas burner diameter of 2–3 m. Not only could break up behavior be investigated, but more importantly flame height data as a function of Q^* could be obtained, particularly for low values of Q^*.

An additional approach to understanding flame height and mass fire behavior would be to perform actual tests closer to the scale of interest. Tests on the order of pool diameters of 100 m would further our knowledge of not only mass fire behavior, but also of fire data, such as surface emissive power, burn rate, and smoke shielding. It is feasible to perform tests spilling volumes up to 200 m^3 (7×10^3 ft^3) resulting in pool diameters up to 100 m (330 ft). Such tests would improve the understanding of

the behavior of large-scale LNG pool fires and would aid in the development and validation of both fundamental and empirical fire models.

Numerical simulation could also be used to gain insight into break up behavior and flame height. The information obtained from experiment at the larger scales, as well as the smaller scale Q^* experiments, would allow for code development and validation. Simulation could then be utilized to help predict behavior at the full scale.

6. Conclusion

The extensive research on LNG thus far has provided significant insight into the physical mechanisms that dominate the dynamics of a spill. The knowledge obtained has also allowed for the development and validation of predictive models that can be used for hazard prediction. The extensive fire testing on hydrocarbon pool fires on land has provided the development of solid flame models. Dispersion tests have allowed for the development of models that incorporate a more complete set of physics. Prior to testing, some of the early Gaussian plume models for dispersion predicted much larger distances to LFL, as much as a factor of 10 or more. Only with experimental data was it possible to improve predictions.

The gaps discussed in this review have indicated several parameters associated with volume released, pool spread and evaporation, dispersion, and pool fires that can significantly affect predicted hazard distances. The uncertainty of these parameters can result in a significant combined affect on thermal hazard predictions. By bringing forth further understanding through testing and simulation, this uncertainty can be substantially reduced.

The approach to field tests should be inclined towards a spill size range that would permit a substantial number of well-instrumented trials allowing for variation of significant parameters in a controlled manner. A few very large tests on the order of $100\,m^3$ ($3.5 \times 10^3\,ft^3$) should be performed, but with the understanding that parameter variation will not be feasible due to the expense of such tests. Performing the larger tests would provide an intermediate scale of data on dispersion and fire, as well as the behavior of rapid phase transitions at these larger scales. Data on smoke shielding and mass fire behavior could also be obtained.

Most imperative is the development of predictive models applicable to the scale involved. Testing at the scales of proposed 'very high consequence events' will never be envisaged due to safety, cost, and feasibility issues. Thus, the only alternative is to utilize models that have been extensively validated, importantly at a scale that represents the physics that occurs at larger scales.

This review has brought out some key areas that require further experimental testing, model development and application. Developing predictive capabilities requires the blending of experimental, numerical, and analytical efforts. With further combined effort on addressing the salient gaps there will be a significant reduction in the uncertainty of current predictive capabilities.

Acknowledgments

The author would like to thank the following individuals for their review and valuable discussion of the manuscript: T. Blanchat, T.Y. Chu, L. A. Gritzo, M. Hightower, and S.R. Tieszen. Sandia is a multiprogram laboratory operated by Sandia Corporation, a Lockheed Martin Company, for the United Stated Department of Energy under Contract DE-AC04-94AL85000.

References

[1] J.A. Fay, Model of spills and fires from LNG and oil tankers, J. Hazard. Mater. 96 (2003) 171–188.
[2] W. Lehr, D. Simecek-Beatty, Comparison of hypothetical LNG and fuel oil fires on water, J. Hazard. Mater. 107 (2004) 3–9.
[3] R.M. Pitblado, J. Baik, G.J. Huges, C Ferro, S.J. Shaw, Consequences of LNG marine incidents, in: Proceedings of the CCPS Conference, Orlando, FL, June 2004.
[4] Quest Consultants, Inc., Modeling LNG Spills in Boston Harbor (2003) 908 26th Ave N.W., Norman, OK 73609; Letter from Quest Consultants to DOE (October 2, 2001); Letter from Quest Consultants to DOE (October 3, 2001); and Letter from Quest Consultants to DOE (November 17, 2003) received by Donald Juckett, Director of the Office of Natural Gas and Petroleum Import and Export Activities until 2003.
[5] J.B. Cornwall, D.W. Johnson, Modeling LNG spills on water, in: AIChE Spring National Meeting, Conference Proceedings, 25–29 April 2004, New Orleans, LA, 2004, pp. 1704–1715.
[6] Final report by the LNG Health and Safety Committee, City of Vallejo, CA, Liquefied Natural Gas in Vallejo: Health and safety issues, January 2003.
[7] Annual Energy Outlook, Energy Information Administration, www.eia.doe.gov.
[8] R.C. Reid, R. Wang, The boiling rates of LNG on typical dike floor materials, Cryogenics (1978) 401–404.
[9] R. Boe, Pool boiling of hydrocarbon mixtures on water, Int. J. Heat Mass Transfer 41 (1998) 1003–1011.
[10] E. Drake, A.A. Jeje, R.C. Reid, Transient boiling of liquefied cryogens on a water surface. II. Light hydrocarbon mixtures, Int. J. Heat Mass Transfer 18 (14) (1975) 1369–1375.
[11] J.A. Valencia-Chavez, R.C. Reid, The effects of composition on the boiling rates of liquefied natural gas for confined spills on water, Int. J. Heat Mass Transfer 22 (1979) 831–838.
[12] C. Conrado, V. Vesovic, The influence of chemical composition on vaporization of LNG and LPG on unconfined water surfaces, Chem. Eng. Sci. 5 (2000) 4549–4562.
[13] Flameless Vapor Explosions, Final Report, LNG Research Center MIT, Cambridge, MA, DOE-OSTI no. 6775451, 1977.
[14] R.P. Anderson, D.R. Armstrong, Experimental study of vapor explosions, in: Proceedings of the Third International Conference on Liquefied Natural Gas, Washington, DC, 1972.
[15] D.L. Katz, D.M. Sliepcevich, LNG: Water explosions, National Academy of Sciences, Report no. CG-D60-74, 1973.
[16] H.C. Goldwire et al. Coyote Series Data Report, LLNL/NWC 1981 LNG Spill Tests Dispersion, Vapor burn and rapid-phase transition, vols. 1 and 2, UCID-19953 Lawrence Livermore National Laboratory, Livermore, California, 1983.
[17] T.G. McRae, et al., Analysis of Large-Scale LNG/Water RPT Explosions, UCRL-91832, Lawrence Livermore National Laboratory, Livermore, California, 1984.
[18] D.L. Morgan, et al., Phenomenology and Modeling of Liquefied Natural Gas Vapor Dispersion, UCRL-53581, Lawrence Livermore National Laboratory, Livermore, California, 1984.
[19] H.C. Rodean, et al., Vapor Burn Analysis for the Coyote Series Lng Spill Experiments, UCRL-53530, Lawrence Livermore National Laboratory, Livermore, California, 1984.

[20] D.L. Ermak, et al., Results of 40 m^3 LNG spills onto water, in: S. Hartwig (Ed.), Heavy Gas and Risk Assessment. II, Battelle-Institute V, Frankfurt am Main, Germany, 1983, pp. 163–179.
[21] D.L. Ermak, et al, LNG spill experiments: dispersion, RPT, and vapor burn analysis, American Gas Assoc. 1982 Operating Section Proc., T203-T209, 1982.
[22] R.P. Koopman, et al., Analysis of Burro series 40 m^3 LNG spill experiments, J. Hazard. Mater. 6 (1982) 43–83.
[23] R.P. Koopman et al., Burro Series Data Report LLNL/NWC 1980 LNG Spill Tests, UCID-19075, Lawrence Livermore National Laboratory, 1982.
[24] T. Enger, D.E. Hartman D.E., LNG spillage on water. II. Final report on rapid phase transitions. Shell Pipeline Corp., Research and Development Laboratory, Houston, Texas, Technical Progress Report No. 1–72, 1972.
[25] B. Jazayeri, Impact cryogenic vapor explosions, M.S. thesis, MIT, Cambridge, Massachusetts, 1975.
[26] G. Berthoud, Vapor Explosions, Annu. Rev. Fluid Mech. 32 (2000) 573–611.
[27] S.A. Schubach, Some aspects of modeling steam explosions, J. Loss Prev. Process Ind. 9 (1996) 193–197.
[28] D.F. Fletcher, T.G. Theofanous, Recent progress in the understanding of steam explosions, J. Loss Prev. Process Ind. 7 (1994) 457–462.
[29] A. Khalil, M.A. Fouad, M.M. Kamel, Modeling of confined cryogenic fuel spills over water, in: Proceedings of the 5th Miami International Symposium on Multi-Phase Transport and Particulate, 1988, pp. 187–199.
[30] W.M. Porteous, M. Blander, Limits of superheat and explosive boiling of light hydrocarbons, halocarbons and hydrocarbon mixtures, AIChE J. 31 (3) (1975) 560–566.
[31] D.H. Napier, D.R. Roochland, Ignition characteristics of rapid phase transition explosions, in: Combustion Institute Canadian Section 1984 Spring Technical Meeting, 1984, pp. 17–19.
[32] B. Otterman, Analysis of large LNG spills on water. Part 1. Liquid spread and evaporation, Cryogenics (1975) 455–460.
[33] C. Georgakis, J. Congalidis, G.C. Williams, Model for non-instantaneous LNG and gasoline spills, Fuel 58 (1979) 113–120.
[34] F. Briscoe, P. Shaw, Spread and evaporation of liquid, Prog. Energy Combust. Sci. 6 (1980) 127–140.
[35] P.K. Raj, A.S. Kalelkar, Assessment models in support of the hazard assessment handbook, U.S. Coast Guard Report No., CC-D-65-74, January 1974.
[36] J.A. Fay, Unusual fire hazard of LNG tanker spills, Comb. Sci. Technol. 7 (1973) 47–49.
[37] D. Hoult, The fire hazard of LNG spilled on water, in: Proceedings of the Conference on LNG Importation and Safety, vol. 87, Boston, MA, 1972.
[38] W.G. May, P.V.K. Perumal, The spreading and evaporation of LNG on water, 74-WA/PID-15, Winter Annual Meeting of ASME, NY, 17–22 November 1974.
[39] G. Opschoor, The spreading and evaporation of LNG- and burning LNG-spills on water, J. Hazard. Mater. 3 (1980) 249–266.
[40] G.J. Boyle, A. Kneebone A., Laboratory investigations into the characteristics of LNG spills on water. Evaporation, spreading and vapor dispersion, Shell Research Ltd., Thornton Research Centre, Report 6-32, March 1973.
[41] D.S. Burgess, J. Biordi, J. Murphy, Hazards associated with the spillage of LNG on water, Report 7448, Bureau of Mines, Pittsburgh, PA, 1970.
[42] D.S. Burgess, J.N. Murphy, M.G. Zabetakis, Hazards of LNG spillage in marine transportation, U.S. Department of Interior, Bureau of Mines, SRS Report No. S4105, February 1970.
[43] P.J. Waite, R.J. Whitehouse, E.B. Winn, W.A. Wakeham, The spread and vaporization of cryogenic liquids on water, J. Hazard. Mater. 8 (1983) 165–184.
[44] J. Brandeis, D.L. Ermak, Numerical simulation of liquefied fuel spills: II. Instantaneous and continuous LNG spills on an unconfined water surface, Int. J. Num. Methods Fluids 3 (1983) 347–361.
[45] T.A. Cavanaugh, J.H. Siegell, K.W. Steinberg, Simulation of vapor emissions from liquid spills, J. Hazard. Mater. 38 (1994) 41–63.
[46] G.F. Feldbauer, J.J. Heigl, W. McQueen, R.H. Whipp, W.G. May, Spills of LNG on water—vaporization and downwind drift of combustible mixtures, API Report EE61E-72, 1972.
[47] W.G. May, W. McQueen, R.H. Whipp, Spills of LNG on water, American Gas Association, Operation Section Proceedings, Paper 73-D-9, 1973.
[48] A.M. Thyer, A review of data on spreading and vaporization of cryogenic liquid spills, J. Hazard. Mater. 99 (2003) 31–40.
[49] F.P. Lees, Loss Prevention in the Process Industries: Hazard Identification, Assessment and Control, vol. 3, second ed., Butterworth-Heinemann, Boston, 1996.
[50] R.C. Reid, J.A. Havens, P.K. Raj, (Eds.), MIT-GRI LNG Safety and Research Workshop, 22–24 March, vol. 1–3, Gas Research Institute, 8600 West Bryn Mawr Ave., Chicago, IL 60631, 1982.
[51] A. Kneebone, L.R. Prew, Shipboard jettison test of LNG onto the sea, in: Proceedings of the 4th International Conference on LNG, Algiers, 1974, pp. 1–25.
[52] J.S. Puttock, D.R. Blackmore, G.W. Colenbrander, Field experiments on dense gas dispersion, J. Hazard. Mater. 6 (1982) 13–41.
[53] D.R. Blackmore, J.A. Eyre, G.G. Summers, Dispersion and combustion behavior of gas clouds resulting from large spillages of LNG and LPG on to the sea, Trans. I. Mar. E. (TM) 94, paper 29, 1982.
[54] D. Blackmore, et al., An updated view of LNG safety, in: American Gas Association Transmission Conference, Operation Section Proceedings, 1982, pp. T226–T232.
[55] G.W. Colenbrander, J.S. Puttock, in: Fourth Int. Sym. on Loss Prev. and Safety, vol. 90, Dense gas dispersion behavior experimental observations and model developments (1983), pp. F66–F76.
[56] R.P. Koopman, et al., Data and calculations on 5 m^3 LNG spill tests, Lawrence Livermore Laboratory, 1978, UCRL-52976.
[57] T.C. Brown et al., Falcon Series Data Report: 1987 LNG Vapor Barrier Verification Field Trials, Final Report, Gas Research Institute, GRI-89/0138, 1990.
[58] S.T. Chan, Numerical simulations of LNG vapor dispersion from a fenced storage area, J. Hazard. Mater. 30 (1992) 195–224.
[59] J.M. Leone et al., FEM3 phase change model, Lawrence Livermore National Laboratory, Report No. UCID-20353, 22, 1985.
[60] S.T. Chan, et al., Numerical simulations of atmospheric releases of heavy gases over variable terrain, in: Air Pollution Modeling and its Applications. III, 1984, pp. 295–328.
[61] S.T. Chan, D.L. Ermak, L.K. Morris, FEM3 model simulations of selected Thorney Island phase 1 trials, J. Hazard. Mater. 16 (1987) 267–292.
[62] D.L. Ermak, S.T. Chan, D.L. Morgan, L.K. Morris, A comparison of dense-gas dispersion model simulations with Burro series LNG spill test results, J. Hazard. Mater. 6 (1982) 129–160.
[63] S.T. Chan, FEM3C: An improved three-dimensional heavy-gas dispersion model: user's manual, UCRL-MA-116567Rev. 1, Lawrence Livermore National Laboratory, December 1994.
[64] S.T. Chan, A three-dimensional model for simulating atmospheric dispersion of heavy-gases over complex terrain, UCRL-JC-127475, Lawrence Livermore National Laboratory September, 1997.
[65] R.I. Sykes, C.P. Cerasoli, D.S. Henn, The representation of dynamic flow effects in a Lagrangian puff dispersion model, J. Hazard. Mater. 64 (1999) 223–247.
[66] R.K.S. Hankin, R.E. Britter, TWODEE: the Health and Safety Laboratory's Shallow Layer Model for Heavy Gas Dispersion. Part 1. Mathematical Basis and Physical Assumptions, J. Hazard. Mater. 66 (1999) 211–226.
[67] R.K.S. Hankin, Heavy gas dispersion: integral models and shallow layer models, J. Hazard. Mater. 102 (2003) 1–10.
[68] D.L. Ermak, User's Manual for SLAB: An atmospheric dispersion model for denser-than-air releases, ACRL-MA-105607, Lawrence Livermore National Laboratory, 1980.
[69] G.W. Colenbrander, J.S. Puttock, Dense gas dispersion behavior experimental observations and model developments, in: Fourth

Int. Sym. on Loss Prev. and Safety, 1983, pp. F66–F75, p. 80.
[70] T.O. Spicer, J.A. Havens, User's guide for the DEGADIS 2.1 dense gas dispersion model environmental protection agency, EPA-450/4-89-019, 1989.
[71] J.A. Havens, Assessment of predictability of LNG vapor dispersion from catastrophic spills onto water, J. Hazard. Mater. 3 (1980) 267–278.
[72] S.R. Hanna, et al., Hazardous gas model evaluation with field observations, Atmos. Environ. 27 (1993) 2265–2285.
[73] P.W.M. Brighton, A.J. Byrne, R.P. Cleaver, P. Courtiade, B. Crabol, R.D. Fitzpatrick, A. Girard, S.J. Jones, V. Lhomme, A. Mercer, D. Nedelka, C. Proux, D.M. Webber, Comparison of heavy gas dispersion models for instantaneous release, J. Hazard. Mater. 36 (1994) 193–208.
[74] B. Carissimo, S.F. Jagger, N.C. Daish, A. Halford, S. Selmer-Olsen, K. Riikonen, J.M. Perroux, J. Wurtz, J.G. Bartzis, N.J. Duijm, K. Ham, M. Schatzmann, R. Hall, The SMEDIS database and validation exercise, Int. J. Environ. Pollut. 16 (2001) 614–629.
[75] N.C. Daish, R.E. Britter, P.F. Linden, S.F. Jagger, B. Carissimo, SMEDIS: scientific model evaluation of dense gas dispersion models, Int. J. Environ. Pollut. 14 (1–6) (2000) 39–51.
[76] http://www.ofcm.noaa.gov/atd_dir/pdf/frontpage.htm.
[77] P.K. Raj et al., Experiments involving pool and vapor fires from spills of liquefied natural gas on water, Arthur D. Little, ADA 077073, June 1979.
[78] A.L. Schneider et al., U.S. Coast Guard Liquefied Natural Gas Research at China Lake, Gastech 78, 5–8 October 1978, Monte Carlo, France, 1979.
[79] P.K. Raj, et al., LNG spill fire tests on water: an overview of the results, Am. Gas Assoc., Oper. Sect., Proc (1979) T246–T251.
[80] A.L. Schneider, Liquefied natural gas spills on water fire modeling, J. Fire Flammability 12 (1980) 302–313.
[81] G.A. Mizner, J.A. Eyre, Radiation from liquefied gas fires on water, Comb. Sci. Technol. 35 (1983) 33–57.
[82] W.J.S. Hirst, J.A. Eyre, Maplin sands experiments 1980: combustion of large LNG and refrigerated liquid propane spills on the sea, Heavy Gas Risk Assess. (1983) 211–224.
[83] P.H. Thomas, The size of flames from natural fires, in: Proceedings of the 9th Int. Combustion Symposium, 1963, pp. 844–859.
[84] H.C. Rodean, et al., Vapor burn analysis for the coyote series LNG spill experiments, Lawrence Livermore National Laboratory, 1984, UCRL-53530.
[85] G.A. Mizner, J. A., Eyre, Large-Scale LNG and LPG Pool Fires, vol. 25, EFCE Publication Series (European Federation of Chemical Engineering), 1982, pp. 147–163.
[86] D. Nedelka, et al., The Montoir 35 m diameter LNG pool fire experiments, in: Int. Conf. Liq. Nat. Gas, vol. 2, 9th, 17–20 October 1989, Nice, France, 1989.
[87] J.R. Welker, C.M. Sleipcevich, Bending of wind-blown flames from liquid pools, Fire Technol. 2 (1966) 127.
[88] P.A. Davies, A guide to the evaluation of condensed phase explosions, J. Hazard. Mater. 33 (1993) 1–33.
[89] J.H.S. Lee, I.O. Moen, The mechanism of transition from deflagration to detonation in vapor cloud explosions, Prog. Energy Combust. Sci. 6 (1980) 359–389.
[90] I.O. Moen, Transition to detonation in fuel-air explosive clouds, J. Hazard. Mater. 33 (1993) 159–192.
[91] M.A. Nettleton, Recent work on gaseous detonations, Shock Waves 12 (2002) 3–12.
[92] D.C. Bull, J.A. Martin, Explosion of unconfined clouds of natural gas, American Gas Association, Transmission Conference, Missouri, USA 16–18th May, AGA Operating Section Proceedings, Paper 77-T-40, 1977.
[93] D.C. Bull, et al., A study of spherical detonation in mixtures of methane and oxygen diluted by nitrogen, J. Phys. D. Appl. Phys. 9 (14) (1976) 1992–2000.
[94] M.C. Parnarouskis et al., Vapor cloud explosion study. Six. Congr. Int. Gaz. Natl. Liq., vol. 2, Sess 3, paper 12, 1980.
[95] C.D. Lind, J.C. Witson, Explosion hazards associated with spills of large quantities of hazardous materials phase II, Report No. CG-D-85-77, 1977.
[96] R. Vander Molen, J.A. Nicholls, Blast wave initiation energy for detonation of methane-ethane-air mixture, Comb. Sci. Technol. 21 (1979) 75–78.
[97] I.O. Moen, et al., Flame acceleration due to turbulence produced by obstacles, Comb. Flame 39 (1980) 21–32.
[98] A.J. Harrison, J.A. Eyre, The effect of obstacle arrays on the combustion of large premixed gas/air clouds, Comb. Sci. Technol. 52 (1987) 121–137.
[99] D. Bradley, T.M. Cresswell, J.S. Puttock, Flame acceleration due to flame-induced instabilities in large-scale explosions, Comb. Flame 124 (2001) 551–559.
[100] S.R. Tieszen, D.W. Stamps, C.K. Westbrook, W.J. Pitz, Gaseous hydrocarbon–air detonations, Comb. Flame 84 (1991) 376–390.
[101] A.L. Schneider, Liquefied-natural gas spills on water-fire modeling, J. Fire Flammability 12 (1980) 302–313.
[102] L.E. Brown, et al., Predict LNG fire radiation, Hydrocarbon Process. (1974) 141–143.
[103] P. Raj, S. Atallah, Thermal radiation from LNG spill fires, Adv. Cryogen. Eng. 20 (1975) 143–150.
[104] R. Lautkaski, Validation of flame drag correlations with data from large pool fires, J. Loss Prev. Process Ind. 5 (1992) 175–180.
[105] A.D. Johnson, A model for predicting thermal radiation hazards from large-scale LNG pool fires, in: Major Hazards Onshore and Offshore, Institute of Chemical Engineers, Symposium Series No. 130, EFCE Event No. 470, EFCE Publication No. 93, Manchester, 20–22 October 1992, pp. 507–524.
[106] E.M. Sparrow, R.D. Hess, Radiation Heat Transfer, Augmented ed., Hemisphere Publishing Corporation, Washington, 1978 (Chapter 4).
[107] P.A. Croce, K.S. Mudan, J. Moorhouse, Thermal radiation from LNG trench fires, vols. 1 and 2, Arthur D. Little, Inc., GRI Report No. 84/0151.1, 1984.
[108] J. Moorhouse, M.J. Pritchard, Thermal radiation hazards from large pool fires and fireballs: a literature review, European Federation of Chemical Engineering 25, Inst. Chem. E. Symp. Ser. 71 (1982) 397–428.
[109] J. Moorhouse, Scaling criteria for pool fires derived from large scale experiments, Int. Chem. E. Symp. Ser. 71 (1982) 165–179.
[110] E.M. Sparrow, A new simpler formulation for radiative angle factors, J. Heat Transfer, Trans., ASME 85 (1963) 81–88.
[111] L.A. Gritzo, S.R. Tieszen, M. Pilch, Establishing the credibility of results from modeled time and length scales in fires, Interflam, in: Proceedings of the 10th International Conference, vol. 2, 2004, pp. 1269–1279.
[112] K.S. Mudan, Thermal radiation hazards from hydrocarbon pool fires, Prog. Energy Combust. Sci. 10 (1984) 59–80.
[113] E.E. Zukoski, Properties of fire plumes, in: G. Cox (Ed.), Combustion Fundamentals of Fire, Academic Press, London, 1995, pp. 101–219.
[114] R.C. Corlett, Velocity distribution in fires, in: P.L. Blackshear (Ed.), Heat Transfer in Fires, John Wiley and Sons, New York, 1974, pp. 239–255.
[115] G. Cox, R. Chitty, Some source-dependent effects of unbounded fires, Comb. Flame 60 (1985) 219–232.
[116] G. Heskestad, Dynamics of the fire plume, Philos. Trans. Soc. Lond. A 356 (1998) 2815–2833.
[117] M.A. Delichatsios, Air entrainment into buoyant jet flames and pool fires, Comb. Flame 70 (1987) 33–46.
[118] G. Heskestad, A reduced-scale mass fire experiment, Comb. Flame 83 (1991) 293–301.
[119] E.E. Zukoski, T. Kubota, B. Cetegen, Entrainment in fire plumes, Fire Saf. J. 3 (1981) 107–121.
[120] H.A. Becker, D. Liang, Visible length of vertical free turbulent diffusion flames comb, Flame 32 (1978) 115.
[121] F.R. Stewart, Prediction of the height of turbulent diffusion buoyant flames, Combust. Sci. Technol. 2 (1970) 203–212.